

Top Polarization in Sbottom Decays at the LHC

Geneviève Bélanger¹, Rohini M. Godbole², Sabine Kraml³, Suchita Kulkarni³

¹ *LAPTH, Université de Savoie, CNRS, B.P.110, F-74941 Annecy-le-Vieux Cedex, France*

² *Centre for High Energy Physics, Indian Institute of Science, Bangalore 560012, India*

³ *Laboratoire de Physique Subatomique et de Cosmologie, UJF Grenoble 1, CNRS/IN2P3, INPG, 53 Avenue des Martyrs, F-38026 Grenoble, France*

Abstract

We perform a comprehensive analysis of the polarization of the top quarks originating from sbottom-pair production at the LHC, followed by sbottom decays to top+chargino. We study moreover the expected net polarization of top quarks produced in sbottom-to-chargino and stop-to-neutralino decays in scenarios with small chargino-neutralino mass difference, where these decays may be hard to distinguish. We show that, in contrast to top quarks produced via Standard Model processes, the average polarization of top quarks originating from these SUSY decays can obtain any value between +1 and -1. We further study the effect of this polarization on the top quark decay kinematics. On the one hand this may be used to construct measures of this polarization, on the other hand it may be used to enhance the search reach in certain scenarios. Exploiting top polarization may also prove useful for searches for “natural” SUSY with light higgsinos, which is typically very difficult to detect at the LHC.

1 Introduction

The discovery of the Higgs boson by both the ATLAS and CMS collaborations [1,2] has provided the last missing piece of the Standard Model (SM). Nevertheless there are still fundamental problems open in the SM, such as the nature of dark matter, the origin of CP violation, or the stability of the electroweak scale, motivating the need for new physics beyond the SM. Supersymmetry (SUSY) is one of the best-motivated extensions of the SM for addressing some of these issues, and the search for supersymmetric particles is thus one of the primary objectives of LHC experiments.

While SUSY searches at the LHC with $\sqrt{s} = 7\text{--}8$ TeV have pushed the mass limits for gluinos and light-flavor squarks beyond 1 TeV, current limits on third generation squarks are much weaker for several reasons. First, the cross section for direct pair production of stops and sbottoms is dominated by gluon-initiated processes and thus drops rapidly as their mass increases. Second, this cross section is much smaller than the total squark–gluino cross section that contributes to the production of SUSY partners of light quarks. Finally, the decays of stops and sbottoms involve some final states with top quarks, which means that the results from the generic $E_T^{\text{miss}} + \text{jets}$ searches are not applicable.

Scenarios with an inverted mass hierarchy, *i.e.* light third but heavy 1st/2nd generation squarks, have hence become a new focus of phenomenological studies. In particular it is interesting to investigate specific signatures of stops and sbottoms as well as methods to determine their properties at the LHC.

Results on stop and sbottom searches in direct pair production are usually quoted in terms of Simplified Model Spectra (SMS), which assume 100% branching ratio in a given channel. The best limit on stops are currently obtained in the $\tilde{t} \rightarrow t\tilde{\chi}_1^0$ channel: based on $\mathcal{L} = 21 \text{ fb}^{-1}$ of data at 8 TeV, the ATLAS collaboration has excluded stops in the mass range 320–680 GeV in the limit of massless neutralinos [3]. Slightly weaker upper limits (600 GeV) are obtained from the channel $\tilde{t} \rightarrow b\tilde{\chi}_1^+$ assuming a small mass difference between the chargino and the neutralino LSP [4], while sbottom masses below 620 GeV are excluded in the channel $\tilde{b} \rightarrow b\tilde{\chi}_1^0$ for neutralino masses below 150 GeV [5] (both results were obtained by the ATLAS collaboration with $\mathcal{L} = 12.8 \text{ fb}^{-1}$). These limits become much weaker with smaller mass splittings between the squark and the neutralino/chargino. Present data therefore allow both top and bottom squarks well below the TeV scale.

For final states involving top quarks, the top polarization can be a useful tool to probe new physics at colliders, as it is sensitive to the helicity structure of the production process (for a recent summary see *e.g.* Ref. [6]). There are different ways to measure the top polarization. In particular, there is a strong correlation between the polarization of the top quark and the angular distributions of its decay leptons. It was shown that this correlation is not affected by higher-order corrections [7–9] or new physics contributions to the decay [10–14]. Measures of top polarization using angular variables have been constructed [13,14] The energy fraction of the decay leptons may also be exploited as a measure of the top polarization [15]. Moreover, it was suggested to make use of boosted top and jet substructure methods in hadronic decays to determine the top polarization [16]. Finally, the determination of the top polarization at the LHC in $t\bar{t}$ events using the angular distributions of the top decay products in the top rest

frame was investigated in [17].

In the SM, pair-produced tops are unpolarized, while singly produced tops have polarization -1 . In SUSY, the polarization of top quarks produced in the decays of stops or sbottoms can take any value between ± 1 , and may provide information on the underlying SUSY scenario. In the context of e^+e^- colliders, the top polarization may be used to probe the mixing in the stop sector [18, 19]. In this case, one can also use the production cross section which depends on the squark mixing. At the LHC, the production cross section is independent of the mixing angle, leaving mainly the polarization to extract information on the stop/sbottom mixing (in addition to branching ratios, if they can be extracted).

Possibilities of measuring the top polarization and hence getting information on the stop mixing in direct stop-pair production at the LHC with $\sqrt{s} = 14$ TeV were investigated in [20, 21]. More generally, in [22] some of us showed how the longitudinal polarization of the top quark from stop decays into neutralinos, $\tilde{t}_1 \rightarrow t\tilde{\chi}_{1,2}^0$, depend on the mixing in both the stop and the neutralino sectors, as well as on the mass difference between the stop and the neutralino. More precisely, for large mass difference $\Delta m = m_{\tilde{t}} - m_{\tilde{\chi}^0} - m_t$, a right-handed (RH) stop produces a negative top polarization when it decays into a higgsino and a positive polarization when it decays into a bino, and vice-versa for a left-handed (LH) stop. On the other hand, the top polarization vanishes in the limit of small Δm . Furthermore, as pointed out in [22, 23], it will affect observables such as the energy distribution of the lepton resulting from the top decay, thus impacting the reach for stop searches at the LHC. In fact, different assumptions about the top polarization are at least in part responsible for the higher reach in the stop mass exclusion by ATLAS (which assumes RH top quarks) than by CMS (which assumes unpolarized top quarks) [24, 25]. Similar effects are expected for sbottom searches in the top+chargino decay channel.

In this paper, we extend the study of [22] by investigating the behavior of the top polarization in sbottom decays into charginos,

$$\tilde{b} \rightarrow t\tilde{\chi}^-.$$

As in the case of stop decays, this polarization may give information on the nature of both the sbottom and the chargino. We will show that for a wino-like chargino the polarization of the top is always -1 , while for a higgsino-like chargino the polarization varies from -1 for a RH sbottom to $+1$ to a LH sbottom. Thus a positive polarization would give indication on the higgsino nature of the chargino. Recall that higgsino-like charginos and neutralinos have small direct production at the LHC and are therefore hard to probe directly especially since the decay products are soft because of the small mass difference between the higgsino states. In reality, the situation is more complicated: when the lighter sbottom \tilde{b}_1 has a large LH component, its mass is similar to that of the lighter stop \tilde{t}_1 (as both are determined by the same soft mass parameter), and therefore tops can come from several different channels, $\tilde{b} \rightarrow t\tilde{\chi}^+$, $\tilde{t} \rightarrow t\tilde{\chi}^0$. At the end, only the net polarization resulting from all different decays will be measurable. Relating the top polarization to the underlying properties of stops, sbottoms and neutralinos/charginos therefore becomes more challenging.

The paper is organized as follows. We summarize our notation and conventions in Section 2 before discussing the fermion polarization in the squark rest frame in Section 3. Polarization-dependent observables are presented in Section 4, and the treatment of the boost in Section 5.

Section 6 contains all numerical results, including the dependence of the polarization on the fundamental SUSY parameters, some benchmark scenarios corresponding to different net polarizations, as well as an analysis of polarization-dependent observables that are relevant for searches at the 14 TeV LHC. Section 7 contains our conclusions.

2 Notation and conventions

For completeness we review in this section our notation and conventions, and give the relevant expressions for sfermion decays into charginos and neutralinos. Overall, we follow the notation of [19], which was also used in [26].

2.1 Sfermion system

Ignoring intergenerational mixing, the sfermion mass matrices can be written as a series of 2×2 matrices, each of which describes sfermions of a specific flavour:

$$\mathcal{M}_{\tilde{f}}^2 = \begin{pmatrix} m_{\tilde{f}_L}^2 & a_f m_f \\ a_f m_f & m_{\tilde{f}_R}^2 \end{pmatrix} = (R^{\tilde{f}})^T \begin{pmatrix} m_{\tilde{f}_1}^2 & 0 \\ 0 & m_{\tilde{f}_2}^2 \end{pmatrix} R^{\tilde{f}} \quad (1)$$

with

$$\begin{aligned} m_{\tilde{f}_L}^2 &= M_L^2 + m_Z^2 \cos 2\beta (I_{3L}^f - e_f \sin^2 \theta_W) + m_f^2, \\ m_{\tilde{f}_R}^2 &= M_R^2 + e_f m_Z^2 \cos 2\beta \sin^2 \theta_W + m_f^2, \\ a_f &= A_f - \mu \{\cot \beta, \tan \beta\}, \end{aligned} \quad (2)$$

for {up, down}-type sfermions; m_f , e_f and I_3^f are the mass, electric charge and the third component of the weak isospin of the partner fermion, respectively; M_L , M_R and A_f are soft SUSY-breaking parameters for each family, and μ is the higgsino mass parameter.

According to eq. (1), $\mathcal{M}_{\tilde{f}}^2$ is diagonalized by a unitary rotation matrix $R^{\tilde{f}}$. The weak eigenstates \tilde{f}_L and \tilde{f}_R are thus related to their mass eigenstates \tilde{f}_1 and \tilde{f}_2 by

$$\begin{pmatrix} \tilde{f}_1 \\ \tilde{f}_2 \end{pmatrix} = R^{\tilde{f}} \begin{pmatrix} \tilde{f}_L \\ \tilde{f}_R \end{pmatrix}, \quad R^{\tilde{f}} = \begin{pmatrix} \cos \theta_{\tilde{f}} & \sin \theta_{\tilde{f}} \\ -\sin \theta_{\tilde{f}} & \cos \theta_{\tilde{f}} \end{pmatrix}. \quad (3)$$

Since the off-diagonal element of $\mathcal{M}_{\tilde{f}}^2$ is proportional to m_f , this mixing is mostly relevant to the third generation, $\tilde{f} = \tilde{t}, \tilde{b}$, on which we concentrate in the following. The mass eigenvalues are given by

$$m_{\tilde{f}_{1,2}}^2 = \frac{1}{2} \left(m_{\tilde{f}_L}^2 + m_{\tilde{f}_R}^2 \mp \sqrt{(m_{\tilde{f}_L}^2 - m_{\tilde{f}_R}^2)^2 + 4(a_f m_f)^2} \right). \quad (4)$$

By convention, we choose \tilde{f}_1 to be the lighter mass eigenstate, $m_{\tilde{f}_1} \leq m_{\tilde{f}_2}$. Notice also that $m_{\tilde{f}_1} \leq m_{\tilde{f}_{L,R}} \leq m_{\tilde{f}_2}$. For the mixing angle $\theta_{\tilde{f}}$ we choose

$$\cos \theta_{\tilde{f}} = \frac{-a_f m_f}{\sqrt{(m_{\tilde{f}_L}^2 - m_{\tilde{f}_1}^2)^2 + (a_f m_f)^2}}, \quad \sin \theta_{\tilde{f}} = \frac{m_{\tilde{f}_L}^2 - m_{\tilde{f}_1}^2}{\sqrt{(m_{\tilde{f}_L}^2 - m_{\tilde{f}_1}^2)^2 + (a_f m_f)^2}}. \quad (5)$$

The \tilde{f}_L - \tilde{f}_R mixing is large if $(m_{\tilde{f}_L}^2 - m_{\tilde{f}_R}^2) \lesssim (a_f m_f)$, with $|\cos \theta_{\tilde{f}}| > \frac{1}{\sqrt{2}}$ if $m_{\tilde{f}_L} < m_{\tilde{f}_R}$ and $|\cos \theta_{\tilde{f}}| < \frac{1}{\sqrt{2}}$ if $m_{\tilde{f}_R} < m_{\tilde{f}_L}$.

2.2 Neutralino system

In the basis

$$\Psi_j^0 = (-i\lambda', -i\lambda^3, \psi_{H_1}^0, \psi_{H_2}^0) \quad (6)$$

the neutralino mass matrix is:

$$\mathcal{M}_N = \begin{pmatrix} M_1 & 0 & -m_Z \sin \theta_W \cos \beta & m_Z \sin \theta_W \sin \beta \\ 0 & M_2 & m_Z \cos \theta_W \cos \beta & -m_Z \cos \theta_W \sin \beta \\ -m_Z \sin \theta_W \cos \beta & m_Z \cos \theta_W \cos \beta & 0 & -\mu \\ m_Z \sin \theta_W \sin \beta & -m_Z \cos \theta_W \sin \beta & -\mu & 0 \end{pmatrix}. \quad (7)$$

The matrix of eq. (7) is diagonalized by the unitary mixing matrix N :

$$N \mathcal{M}_N N^T = \text{diag}(m_{\tilde{\chi}_1^0}, m_{\tilde{\chi}_2^0}, m_{\tilde{\chi}_3^0}, m_{\tilde{\chi}_4^0}), \quad (8)$$

where $m_{\tilde{\chi}_n^0}$, $n = 1, \dots, 4$, are the (non-negative) masses of the physical neutralino states with $m_{\tilde{\chi}_1^0} < \dots < m_{\tilde{\chi}_4^0}$.

2.3 Chargino system

The chargino mass matrix is:

$$\mathcal{M}_C = \begin{pmatrix} M_2 & \sqrt{2} m_W \sin \beta \\ \sqrt{2} m_W \cos \beta & \mu \end{pmatrix}. \quad (9)$$

It is diagonalized by two unitary matrices U and V ,

$$U \mathcal{M}_C V^T = \text{diag}(m_{\tilde{\chi}_1^\pm}, m_{\tilde{\chi}_2^\pm}), \quad (10)$$

where $m_{\tilde{\chi}_{1,2}^\pm}$ are the masses of the physical chargino states with $m_{\tilde{\chi}_1^\pm} < m_{\tilde{\chi}_2^\pm}$.

2.4 Sfermion interaction with charginos and neutralinos

The sfermion interactions with charginos, which will define the $\tilde{b} \rightarrow t\tilde{\chi}^-$ decays, are

$$\mathcal{L}_{f\tilde{f}\tilde{\chi}^\pm} = g\bar{u}(l_{ij}^{\tilde{d}}P_R + k_{ij}^{\tilde{d}}P_L)\tilde{\chi}_j^+\tilde{d}_i + g\bar{d}(l_{ij}^{\tilde{u}}P_R + k_{ij}^{\tilde{u}}P_L)\tilde{\chi}_j^{+c}\tilde{u}_i + \text{h.c.} \quad (11)$$

where $i, j = 1, 2$, u (\tilde{u}) stands for up-type (s)quark, and d (\tilde{d}) stands for down-type (s)quark, g is the SU(2) coupling constant. The coupling matrices $l^{\tilde{f}}$ and $k^{\tilde{f}}$ are

$$l_{ij}^{\tilde{t}} = -V_{j1}R_{i1}^{\tilde{t}} + h_t V_{j2}R_{i2}^{\tilde{t}}, \quad l_{ij}^{\tilde{b}} = -U_{j1}R_{i1}^{\tilde{b}} + h_b U_{j2}R_{i2}^{\tilde{b}}, \quad (12)$$

$$k_{ij}^{\tilde{t}} = h_b U_{j2}R_{i1}^{\tilde{t}}, \quad k_{ij}^{\tilde{b}} = h_t V_{j2}R_{i1}^{\tilde{b}}, \quad (13)$$

for stops and sbottoms, with the Yukawa couplings h_f given by

$$h_t = \frac{m_t}{\sqrt{2}m_W \sin \beta}, \quad h_b = \frac{m_b}{\sqrt{2}m_W \cos \beta}. \quad (14)$$

The sfermion interactions with neutralinos are ($i = 1, 2$; $n = 1, \dots, 4$)

$$\begin{aligned} \mathcal{L}_{f\tilde{f}\tilde{\chi}^0} &= g\bar{f}(f_{Ln}^{\tilde{f}}P_R + h_{Ln}^{\tilde{f}}P_L)\tilde{\chi}_n^0\tilde{f}_L + g\bar{f}(h_{Rn}^{\tilde{f}}P_R + f_{Rn}^{\tilde{f}}P_L)\tilde{\chi}_n^0\tilde{f}_R + \text{h.c.} \\ &= g\bar{f}(a_{in}^{\tilde{f}}P_R + b_{in}^{\tilde{f}}P_L)\tilde{\chi}_n^0\tilde{f}_i + \text{h.c.} \end{aligned} \quad (15)$$

where

$$a_{in}^{\tilde{f}} = f_{Ln}^{\tilde{f}}R_{i1}^{\tilde{f}} + h_{Rn}^{\tilde{f}}R_{i2}^{\tilde{f}}, \quad (16)$$

$$b_{in}^{\tilde{f}} = h_{Ln}^{\tilde{f}}R_{i1}^{\tilde{f}} + f_{Rn}^{\tilde{f}}R_{i2}^{\tilde{f}}. \quad (17)$$

The $f_{L,R}^{\tilde{f}}$ and $h_{L,R}^{\tilde{f}}$ couplings are

$$\begin{aligned} f_{Ln}^{\tilde{t}} &= -\frac{1}{\sqrt{2}}(N_{n2} + \frac{1}{3}\tan\theta_W N_{n1}), & f_{Ln}^{\tilde{b}} &= \frac{1}{\sqrt{2}}(N_{n2} - \frac{1}{3}\tan\theta_W N_{n1}), \\ f_{Rn}^{\tilde{t}} &= \frac{2\sqrt{2}}{3}\tan\theta_W N_{n1}, & f_{Rn}^{\tilde{b}} &= -\frac{\sqrt{2}}{3}\tan\theta_W N_{n1}, \\ h_{Rn}^{\tilde{t}} &= -h_t N_{n4} = h_{Ln}^{\tilde{t}*}, & h_{Rn}^{\tilde{b}} &= -h_b N_{n3} = h_{Ln}^{\tilde{b}*} \end{aligned} \quad (18)$$

for stops ($\tilde{f} = \tilde{t}$) on the left and sbottoms ($\tilde{f} = \tilde{b}$) on the right.

3 Fermion polarization in the sfermion rest frame

For a sfermion decaying into a chargino or a neutralino, the gaugino interaction conserves the helicity of the sfermion while the higgsino interaction flips it. We define the average polarisation of the produced fermions as

$$P_f = \frac{\sigma(+, +) - \sigma(-, -)}{\sigma(+, +) + \sigma(-, -)}, \quad (19)$$

where $\sigma(\pm, \pm)$ is the cross section for a positive or negative helicity fermion respectively. In general one expects non trivial polarization effects only for the third generation fermions, furthermore only the polarization of the top quark or the τ can be measured. In this paper we will discuss only the top polarization.

3.1 $\tilde{b} \rightarrow t\tilde{\chi}^-$ decays

For tops coming from $\tilde{b}_i \rightarrow t\tilde{\chi}_j^-$ decays, the polarisation given by eq. (19), is

$$\mathcal{P}_t = \frac{[(k_{ij}^{\tilde{b}})^2 - (l_{ij}^{\tilde{b}})^2] f_1}{(k_{ij}^{\tilde{b}})^2 + (l_{ij}^{\tilde{b}})^2 - 2k_{ij}^{\tilde{b}} l_{ij}^{\tilde{b}} f_2}, \quad (20)$$

with the factors f_1 and f_2 , purely kinematical in origin, given by

$$f_1 = m_t \frac{(p_{\tilde{\chi}_j^-} \cdot s_t)}{(p_t \cdot p_{\tilde{\chi}_j^-})}, \quad f_2 = m_t \frac{m_{\tilde{\chi}_j^-}}{(p_t \cdot p_{\tilde{\chi}_j^-})}. \quad (21)$$

Here m_t , p_t and s_t denote the top mass, momentum and longitudinal spin vector, respectively, and $p_{\tilde{\chi}_j^-}$ is the momentum of the chargino. In the rest frame of the decaying sbottom, these factors become

$$f_1 = \frac{\lambda^{\frac{1}{2}}(m_{\tilde{b}_i}^2, m_t^2, m_{\tilde{\chi}_j^-}^2)}{m_{\tilde{b}_i}^2 - m_{\tilde{\chi}_j^-}^2 - m_t^2}, \quad f_2 = \frac{2m_t m_{\tilde{\chi}_j^-}}{m_{\tilde{b}_i}^2 - m_{\tilde{\chi}_j^-}^2 - m_t^2}, \quad (22)$$

with the function λ defined as

$$\lambda(x, y, z) = x^2 + y^2 + z^2 - 2xy - 2yz - 2xz. \quad (23)$$

The factors $f_1 \rightarrow 1$ and $f_2 \rightarrow 0$ if m_t was negligible. Moreover, for large $\Delta m \equiv m_{\tilde{b}_i} - m_{\tilde{\chi}_j^-} - m_t$, $f_1 \rightarrow 1$ irrespective of m_t . For $\tilde{b}_1 \rightarrow t\tilde{\chi}^-$ decays, we have

$$\begin{aligned} (k_{1j}^{\tilde{b}})^2 - (l_{1j}^{\tilde{b}})^2 &= h_t^2 V_{j2}^2 \cos^2 \theta_{\tilde{b}} - (h_b U_{j2} \sin \theta_{\tilde{b}} - U_{j1} \cos \theta_{\tilde{b}})^2 \\ &= (h_t^2 V_{j2}^2 - U_{j1}^2) \cos^2 \theta_{\tilde{b}} - h_b^2 U_{j2}^2 \sin^2 \theta_{\tilde{b}} + h_b U_{j1} U_{j2} \sin 2\theta_{\tilde{b}}. \end{aligned} \quad (24)$$

For \tilde{b}_2 decays, the corresponding expression $(k_{2j}^{\tilde{b}})^2 - (l_{2j}^{\tilde{b}})^2$ is given by the RHS of eq. (24) with $\cos^2 \theta_{\tilde{b}}$, $\sin^2 \theta_{\tilde{b}}$ interchanged, and a change in sign of the term $\propto \sin 2\theta_{\tilde{b}}$.

It is interesting to consider certain limiting cases for the $\tilde{b}_1 \rightarrow t\tilde{\chi}_1^-$ decay. For $M_2 \ll |\mu|$, the chargino is **wino-like**, and the mixing matrices U and V are given by:¹

$$U \rightarrow \begin{pmatrix} -1 & 0 \\ 0 & 1 \end{pmatrix}, \quad V \rightarrow \begin{pmatrix} -1 & 0 \\ 0 & 1 \end{pmatrix}. \quad (25)$$

The resulting top polarization \mathcal{P}_t is then:

$$\mathcal{P}_t = \frac{-(l_{11}^{\tilde{b}})^2 f_1}{(l_{11}^{\tilde{b}})^2} = -f_1. \quad (26)$$

¹Up to an overall phase.

Therefore, for large enough Δm , we expect $\mathcal{P}_t \simeq -1$ in case of a pure wino-like chargino, irrespective of the sbottom mixing angle. (It should be noted however that in practice for the range of parameters we will be considering all entries of the matrices U and V are non-zero and will be taken into account.)

For a **higgsino-like** chargino, i.e. $|\mu| \ll M_2$, the mixing matrices U and V approach

$$U \rightarrow \begin{pmatrix} 0 & 1 \\ 1 & 0 \end{pmatrix}, \quad V \rightarrow \begin{pmatrix} 0 & 1 \\ 1 & 0 \end{pmatrix}, \quad (27)$$

and the resulting top polarization is

$$\mathcal{P}_t = \frac{((h_t \cos \theta_{\tilde{b}})^2 - (h_b \sin \theta_{\tilde{b}})^2) f_1}{[(h_t \cos \theta_{\tilde{b}})^2 + (h_b \sin \theta_{\tilde{b}})^2 - h_t h_b \sin 2\theta_{\tilde{b}}] f_2}. \quad (28)$$

Therefore, for a higgsino-like chargino, the top polarization depends on the sbottom mixing. In the limit of pure LH or RH sbottoms we have

$$\tilde{b}_L : \cos \theta_{\tilde{b}} = 1, \quad \mathcal{P}_t \rightarrow +f_1, \quad (29)$$

$$\tilde{b}_R : \cos \theta_{\tilde{b}} = 0, \quad \mathcal{P}_t \rightarrow -f_1. \quad (30)$$

In other words, a wino-like chargino, whose interaction conserves chirality, couples to a left-chiral sbottom and a left-handed top (recall that just like the W^\pm , a wino has only left-chiral interactions) thus always giving a top polarization close to -1 , similar to single top production in the SM. The higgsino interaction, on the other hand, flips chirality and couples a right (left) chiral sbottom to a left (right) handed top; the top polarization thus can vary from -1 to $+1$ depending on the sbottom mixing angle and the bottom Yukawa coupling, which becomes relevant at large $\tan \beta$. This will be discussed in more detail in Section 6.

3.2 $\tilde{t} \rightarrow t\tilde{\chi}^0$ decays

For completeness we also summarize the case of stop decays into neutralinos, c.f. [26]. Analogous to eq. (20), the average top polarization from $\tilde{t}_i \rightarrow t\tilde{\chi}_n^0$ is given by

$$\mathcal{P}_t = \frac{[(b_{in}^{\tilde{t}})^2 - (a_{in}^{\tilde{t}})^2] f_1}{(b_{in}^{\tilde{t}})^2 + (a_{in}^{\tilde{t}})^2 - 2b_{in}^{\tilde{t}} a_{in}^{\tilde{t}} f_2} \quad (31)$$

with the obvious replacement $p_{\tilde{\chi}_j^-} \rightarrow p_{\tilde{\chi}_n^0}$ in eq. (21). Using eqs. (16), (17) and (3), the stop couplings are written as

$$\begin{aligned} a_{1n}^{\tilde{t}} &= -\frac{1}{\sqrt{2}} \left(N_{n2} + \frac{1}{3} \tan \theta_W N_{n1} \right) \cos \theta_{\tilde{t}} - h_t N_{n4} \sin \theta_{\tilde{t}} \\ b_{1n}^{\tilde{t}} &= \frac{2\sqrt{2}}{3} \tan \theta_W N_{n1} \sin \theta_{\tilde{t}} - h_t N_{n4}^* \cos \theta_{\tilde{t}} \end{aligned} \quad (32)$$

Substituting these in the expression for the polarization, eq. (31), one easily sees that in the case of large mass differences between the stop and the neutralino ($f_1 \rightarrow 1$) a RH stop will lead to $\mathcal{P}_t = -1$ when it decays into a higgsino and to $\mathcal{P}_t = +1$ when the decay is into a gaugino; a LH stop will lead to the opposite polarizations.

4 Effect of top polarization on the decay kinematics

The $V - A$ interaction involved in the decay of the top quark, $t \rightarrow Wb \rightarrow i i' b$, where i and i' denote the decay products of the W , implies definite correlations between the direction of top spin and the top decay products. These are most clearly understood in the rest frame of the top quark. Since the top decays before it hadronises, these correlations are not washed out by the hadronisation process. We discuss explicitly only the case of the top, given that top and anti-top can be distinguished by the charge of the decay lepton. Note also that we neglect the effect of the off-diagonal elements of the CKM matrix and use $BR(t \rightarrow Wb) = 1$.

Consider a top quark ensemble with degree of polarization \mathcal{P}_t . In the top quark rest frame, the angular distribution of the decay product f is given by:

$$\frac{1}{\Gamma_t} \frac{d\Gamma_l}{d \cos \theta_{f,\text{rest}}} = \frac{1}{2} (1 + \kappa_f \mathcal{P}_t \cos \theta_{f,\text{rest}}), \quad (33)$$

where Γ_t is the partial decay width of the top and $\theta_{f,\text{rest}}$ denotes the angle between the momentum of the f and the top spin vector. κ_f is called analyzing power of the decay product f [27]. It is 1 for a positively charged lepton or a d quark. For a u quark or ν_l , $\kappa_{u,\nu} = -0.31$, while for b and W the values are $\kappa_b = -0.4$ and $\kappa_W = 0.4$, respectively. The maximal value of $\kappa_l = 1$ means that the charged lepton is the most efficient polarisation analyzer. Corrections to the values of κ_f can originate from any deviation of the tbW coupling from the standard $V - A$ structure and/or from higher order QCD and QED corrections. The leading QCD corrections to κ_b , κ_d and κ_u are of the order of a few percent, somewhat decreasing its magnitude [9]. The values of κ_l and κ_d on the other hand do not receive any corrections from the anomalous tbW coupling at leading order [14]. Hence the angular distribution of the decay lepton in the rest frame reflects the polarization of the decaying top quark faithfully, even in the presence of such anomalous couplings. Thus it is an unambiguous measure of top polarization effects.

It is also interesting to consider how polarization affects the kinematic distributions of the top decay products in the laboratory frame. This allows to construct useful polarization-dependent observables. The use of laboratory observables to measure top polarization would obviate the need for reconstruction of the top rest frame. This is desirable as such a reconstruction may not be always possible. The correlation between the polarization of the top and the different kinematic variables of the decay products can be obtained from eq. (33) and appropriate Lorentz transformations. Just like the angular distribution in the top rest frame, the energy integrated decay lepton angular distributions in the laboratory frame are also unaltered to linear order in the anomalous tbW coupling [10–14]. For all the other distributions, including the energy distribution of the decay lepton, a deviation of the distribution from the unpolarized case can not be uniquely attributed to the top polarization.

While constructing polarization dependent observables, it is worth recalling that the decay product distributions in the lab frame are influenced not only by the top quark polarization, but also by the boost β_t from the top-quark rest frame to the laboratory frame and by the transverse momentum p_t^T of the top quark. Here we will use a boost parameter based on the

total momentum of the top $|\vec{p}_t|$ and the top energy E_t

$$\beta_t = \frac{|\vec{p}_t|}{E_t}. \quad (34)$$

As an example we consider the lab-frame polar angle θ_l of the lepton w.r.t. the top quark direction. Due to the top boost, θ_l is smaller than its counterpart in the rest frame $\theta_{l,\text{rest}}$. Thus, the distribution of θ_l in the lab frame is more strongly peaked towards 0 for a stronger top boost as well as for a more positively polarized top quark. One can then define a polar angle asymmetry A_{θ_l} as

$$A_{\theta_l} = \frac{\sigma(\theta_l < \pi/4) - \sigma(\theta_l > \pi/4)}{\sigma(\theta_l < \pi/4) + \sigma(\theta_l > \pi/4)}. \quad (35)$$

In addition to the polar angle, one can study the azimuthal angle distribution. To this end, we choose the proton beam direction as the z -axis and define the top production plane as the $x - z$ plane. Moreover, we identify the positive x component with the direction of the top quark. At the LHC, since the initial state has identical particles, the z -axis can point in the direction of either proton. This symmetry implies that one cannot distinguish between an azimuthal angle ϕ and an angle $2\pi - \phi$. In the rest frame this variable does not depend on the longitudinal polarization, but in the lab frame it picks up a dependence on $\theta_{l,\text{rest}}$ through the top boost. For positively polarized tops it is peaked at $\phi_l = 0$ and $\phi_l = 2\pi$, with a minimum at $\phi_l = \pi$ [13, 14]. It should be noted that nonzero p_t^T also causes the ϕ_l distributions to peak near $\phi_l = 0$ and $\phi_l = 2\pi$, *independent* of the polarization state of the t quark. In other words, the peaking at $\phi_l = 0$ and 2π is caused by kinematic effects, even for an unpolarized top. It is enhanced even further for a positively polarized top. For a completely negatively polarized top, the pure polarization dependent effects can sometimes even overcome the peaking caused by kinematical effects. The peaks of the distribution then shift a little away from $\phi = 0$ and 2π . More importantly they lie below those expected for the positively polarized and unpolarized top. The relative number of leptons near $\phi = 0$ and 2π is thus reduced progressively as we go from a positively polarized to unpolarized to a negatively polarized top. For normalized distributions the ordering is exactly the opposite at $\phi = \pi$ where the relative number of leptons increases as we go from a positively polarized top to a negatively polarized top. This shape then motivates the definition of the azimuthal angle asymmetry [14]:

$$A_{\phi_l} = \frac{\sigma(\cos \phi_l > 0) - \sigma(\cos \phi_l < 0)}{\sigma(\cos \phi_l > 0) + \sigma(\cos \phi_l < 0)}, \quad (36)$$

where σ is the fully integrated cross section. Note that a higher top polarization or a stronger top boost will result in a more sharply peaked ϕ_l distribution and thus yield a larger asymmetry.

It is also useful to consider energy observables. Although they are not completely independent of an anomalous tbW coupling as mentioned above, they do carry information about the top polarization. In fact, for a positively polarized top, the energy and the transverse momentum distributions for the lepton are shifted to higher values as compared to the unpolarized

or negatively polarized case. Since top quarks produced from SM processes are either unpolarized or negatively polarized, this feature of the E_l and p_T^l distributions for positively polarized top quarks can provide an effective discrimination against the SM background. Since the κ_b and κ_l have opposite signs, the effect of top polarization on the energy and p_T distributions of the b -jet in the laboratory frame is exactly in the opposite direction to that for the lepton distributions. In Ref. [28], this feature was employed in constructing a discriminator of top quark polarization using the p_T of the b -quark. Furthermore, the energy distribution can be of particular use when the top quarks are highly boosted. In this case, the effect of the boost on the angular distribution may mask the polarization and an accurate determination of the angles (for asymmetries) may be difficult. It was shown in [29] that in a kinematic regime where the tops are heavily boosted, the ratios

$$z = \frac{E_b}{E_t}, \quad u = \frac{E_l}{E_l + E_b}, \quad (37)$$

are sensitive to the polarization state of the top quark. Here E_t , E_b and E_l are respectively the (lab frame) energies of the top quark, and of the b quark and lepton coming from its decay. The analysis of [29] was at the LO parton level, but in practical applications one may also consider E_b to be the energy of *e.g.* a b jet. Note that the ranges of z and u are given in principle by

$$0 \leq z, u \leq 1, \quad (38)$$

although there will be a cut-off at high and low values due to the finite b quark and W boson masses. In the collinear limit $\beta_t = 1$, the normalized distribution $\frac{1}{\Gamma} \frac{d\Gamma}{dz}$ can be in fact computed analytically [29]. It is peaked at lower values of z for a positively polarized tops, and at high values of z for negatively polarized tops. In case of the u distribution, which has to be computed numerically, even in the $\beta_t = 1$ limit, the peak is shifted by about 0.1 for $\mathcal{P}_t = -1$ compared to the unpolarized case; whereas for $\mathcal{P}_t = 1$ the normalized distribution is weighted towards larger values of u . One can of course define these observables for any value of a cut on the top boost. However, at low boost values, both z and u are increasingly contaminated with contributions that are independent of \mathcal{P}_t , thus reducing their effectiveness as discriminators of top polarization and/or new physics parameters. We will show later how these distributions may be exploited for quantitative measures of polarization.

5 Boost treatment

Before proceeding to the numerical analysis, we find it useful to give some details on the treatment of the boost. Note that the overall boost of the top quark in the laboratory frame depends on the boost of the sfermion, that of the top in the sfermion rest frame and the angle of emission of the top with respect to the sfermion. As a consequence, the relation between the top polarization in the sfermion rest frame, discussed in Sections 3 and 6.1, and the top polarization measured in the lab frame depends on all these.

We explain the procedure we have used to obtain the top quark polarization in the lab frame with the concrete example of $\tilde{b}_1 \rightarrow t\tilde{\chi}_1^-$ decays. The same treatment will later be applied to all other decays, including stop decays to top+neutralino, in order to obtain the total polarization from all sbottom and stop decays into tops, *i.e.* the quantity that is actually relevant for experiment.

First, we define our frame of reference such that the decaying sbottom is at rest and the top momentum lies in the $x - z$ plane. In this frame, the momentum vectors of the sbottom, top and chargino are defined as:

$$\begin{aligned} p_{\tilde{b}_1} &= (m_{\tilde{b}_1}, 0, 0, 0) \\ p_t &= (E_t, |p_t| \sin \vartheta, 0, |p_t| \cos \vartheta) = (E_t, p_{tx}, 0, p_{tz}) \\ p_{\tilde{\chi}_1^-} &= (E_{\tilde{\chi}_1^-}, -|p_t| \sin \vartheta, 0, -|p_t| \cos \vartheta) \end{aligned} \quad (39)$$

where, ϑ is the angle between decaying top and chargino and $|p_t|$ is the magnitude of the top momentum given by:

$$|p_t| = \frac{\lambda^{\frac{1}{2}}(m_{\tilde{b}_1}^2, m_t^2, m_{\tilde{\chi}_1^\pm}^2)}{2m_{\tilde{b}_1}} \quad (40)$$

Furthermore, we specify the z -component of the top spin vector as:²

$$s_t^3 = \left(\frac{|p_t|}{m_t}, \frac{E_t}{m_t} \frac{p_{tx}}{|p_t|}, 0, \frac{E_t}{m_t} \frac{p_{tz}}{|p_t|} \right) \quad (41)$$

The top-polarization in terms of helicity amplitude formalism is defined as:

$$\begin{aligned} \mathcal{P}_t &= \frac{\int \frac{d\sigma(+,+)}{d\cos\vartheta} d\cos\vartheta - \int \frac{d\sigma(-,-)}{d\cos\vartheta} d\cos\vartheta}{\int \frac{d\sigma(+,+)}{d\cos\vartheta} d\cos\vartheta + \int \frac{d\sigma(-,-)}{d\cos\vartheta} d\cos\vartheta} \\ &= \frac{(k_{ij}^2 - l_{ij}^2) \int m_t (p_{\tilde{\chi}_1^-} \cdot s_t^3) d\cos\vartheta}{(k_{ij}^2 + l_{ij}^2) \int (p_t \cdot p_{\tilde{\chi}_1^-}) d\cos\vartheta - 2k_{ij} l_{ij} \int m_t m_{\tilde{\chi}_1^-} d\cos\vartheta} \end{aligned} \quad (42)$$

Now we boost the system in the positive z -direction. Note that the spin vector s_t^3 is not a Lorentz vector, hence the dot product $(p_{\tilde{\chi}_1^-} \cdot s_t^3)$ is not Lorentz invariant. Thus, the resulting top polarization has a dependence on the boost.

²Since we are interested in the longitudinal polarization of the top, we are not concerned about the spin vectors in the x and y directions.

6 Numerical analysis

For the numerical analysis, we choose to work within the framework of the general R-parity and CP conserving MSSM with parameters defined at the electroweak scale. The relevant soft terms for our analysis are the left and right 3rd generation soft masses $M_{\tilde{Q}_3}$, $M_{\tilde{U}_3}$, $M_{\tilde{D}_3}$ and the trilinear couplings A_t , A_b entering the stop and sbottom mass matrices, together with the gaugino masses M_1 and M_2 , the higgsino mass parameter μ , and $\tan\beta$. The top quark mass is fixed at 173.2 GeV.

We consider the two cases of higgsino-like or wino-like $\tilde{\chi}_1^\pm$. For the example of a higgsino-like chargino, we set $\mu = 350$ GeV and $M_2 = 1000$ GeV; the neutralino sector is fixed by $M_1 = 500$ GeV. This gives $m_{\tilde{\chi}_1^\pm} \simeq 352$ GeV, $m_{\tilde{\chi}_2^0} \simeq 358$ GeV and $m_{\tilde{\chi}_1^0} \simeq 343$ GeV (for $\tan\beta = 10$, but showing only little variation with $\tan\beta$). For the wino-like case, we reverse the parameters, setting $M_2 = 350$ GeV and $\mu = 1000$ GeV. With $M_1 = 250$ GeV, this gives $m_{\tilde{\chi}_1^\pm} \simeq m_{\tilde{\chi}_2^0} \simeq 360$ GeV and $m_{\tilde{\chi}_1^0} \simeq 247$ GeV.³

In general, we use `SoftSUSY` [30] to compute the full MSSM spectrum. However, when considering only the $\tilde{b}_1 \rightarrow \tilde{\chi}_1^- t$ decay, we directly take the lighter sbottom mass, $m_{\tilde{b}_1}$, and the sbottom mixing angle, $\cos\theta_{\tilde{b}}$, as free parameters; the exact values of the stop/sbotttom soft terms are not necessary in this case. For computing sparticle decays, checking flavor observables, etc., we use `micrOMEGAs` [31, 32]. Cross sections are computed at NLO with `Prospino` [33]. Finally, for generating distributions, we use `MadGraph` [34, 35] with v4 model files.

6.1 Parameter dependencies for \tilde{b}_1

Let us first discuss the results for top polarization in the sbottom rest frame. Figure 1 shows the polarization of the top quark coming from the $\tilde{b}_1 \rightarrow \tilde{\chi}_1^- t$ decay as a function of the sbottom mixing angle, for the case of large Δm ; concretely we take $m_{\tilde{b}_1} = 685$ GeV and, as mentioned above, $\mu = 350$ GeV and $M_2 = 1000$ GeV ($M_2 = 350$ GeV and $\mu = 1000$ GeV) for the higgsino (wino) case, with $M_1 = 500$ GeV. As discussed in Section 3.1, for a wino-like chargino the polarization of the top is always ≈ -1 regardless of the nature of the decaying sbottom. For a higgsino-like chargino, on the other hand, \mathcal{P}_t varies from -1 for a \tilde{b}_L to $+1$ for a \tilde{b}_R . For small $\tan\beta$, i.e. small bottom Yukawa coupling, the transition happens very quickly around $\cos\theta_{\tilde{b}} \sim 0.1 - 0.25$. For large $\tan\beta$, where top and bottom Yukawa couplings are equally important, the transition happens more slowly and for maximally mixed sbottoms; as a result, all values of $\mathcal{P}_t \in [-1, +1]$ can be easily obtained without having to fine-tune the value of the sbottom mixing angle. We also note that for $\cos\theta_{\tilde{b}} = 0$, $\mathcal{P}_t = -0.92$; when $\cos\theta_{\tilde{b}}$ slightly increases above zero, the top Yukawa coupling starts playing a role in the denominator of eq. (28), causing \mathcal{P}_t to first decrease to -1 before increasing to $+1$ for larger $\cos\theta_{\tilde{b}}$. A similar effect can be seen for $\cos\theta_{\tilde{b}} \approx 1$: $\mathcal{P}_t = +1$ is obtained for $\cos\theta_{\tilde{b}} = 0.7$, while at $\cos\theta_{\tilde{b}} = 1$, $\mathcal{P}_t = 0.945$.

³When the rest of the SUSY spectrum is needed, we set the slepton soft terms to $M_{\tilde{L}_i} = M_{\tilde{R}_i} = 500$ GeV ($i = 1..3$), the squark soft terms of the first two generations to $M_{\tilde{Q}_j} = M_{\tilde{U}_j} = M_{\tilde{D}_j} = 2$ TeV ($j = 1, 2$), the gluino soft mass $M_3 = 1.5$ TeV, and the pseudoscalar Higgs mass $m_A = 1.5$ TeV. The right stop mass parameter $M_{\tilde{U}_3}$ and the trilinear coupling A_t are adjusted such that $m_h \approx 126$ GeV.

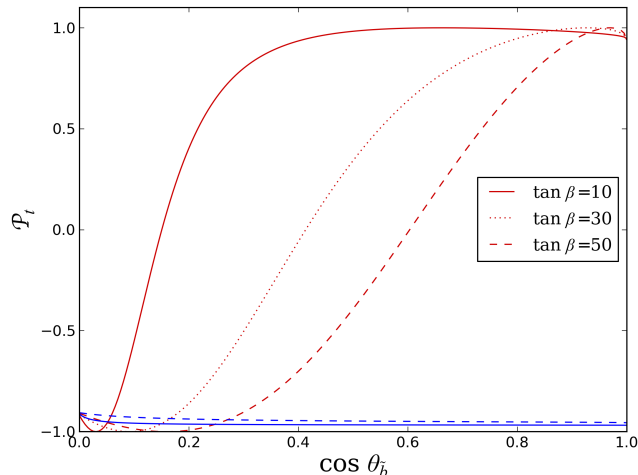


Figure 1: Top polarization in $\tilde{b}_1 \rightarrow \tilde{\chi}_1^- t$ decays as a function of the sbottom mixing angle, for $m_{\tilde{b}_1} = 685$ GeV. For the higgsino-like case $\mu = 350$ GeV and $M_2 = 1000$ GeV (in red), while for the wino-like case $M_2 = 350$ GeV and $\mu = 1000$ GeV (in blue). The solid, dotted, and dashed lines are for $\tan \beta = 10, 30,$ and $50,$ respectively.

In order to understand the dependence of \mathcal{P}_t on the relative strength of the Yukawa couplings, let us simplify eq. (20) for a completely higgsino-like chargino, cf. eq. (28). We get

$$\mathcal{P}_t = \frac{\left(\frac{\cos^2 \theta_{\tilde{b}}}{\sin^2 \theta_{\tilde{b}}} - \frac{h_b^2}{h_t^2} \right) f_1}{\left(\frac{\cos^2 \theta_{\tilde{b}}}{\sin^2 \theta_{\tilde{b}}} + \frac{h_b^2}{h_t^2} \right) - 2 \frac{\cos \theta_{\tilde{b}}}{\sin \theta_{\tilde{b}}} \frac{h_b}{h_t} f_2} \quad (43)$$

Now recall that $f_1 \simeq 1$ away from the kinematic boundary, while $f_2 \rightarrow 0$. Hence, for $\cos^2 \theta_{\tilde{b}} / \sin^2 \theta_{\tilde{b}} > h_b^2 / h_t^2$, $\mathcal{P}_t > 0$ and for $\cos^2 \theta_{\tilde{b}} / \sin^2 \theta_{\tilde{b}} < h_b^2 / h_t^2$, $\mathcal{P}_t < 0$. This effect is illustrated in Fig. 2. Also, for a fixed value of $\cos \theta_{\tilde{b}}$, $|\mathcal{P}_t|$ decreases with increasing $\tan \beta$.

The dependence on the available phase space, Δm , is illustrated in Fig. 3. The left panel shows the case of a higgsino-like chargino while the right panel shows the wino-like case. The top polarization as described in eq. (20) is directly proportional to f_1 , which goes to zero when $\Delta m \rightarrow 0$ and, as a result, $\mathcal{P}_t \rightarrow 0$. This can very well be seen in both the higgsino-like and the wino-like scenarios. Away from the kinematic boundary, $f_1 \rightarrow 1$ and $f_2 \rightarrow 0$. For $\Delta m > 100$ GeV, f_1 is very near 1 and the polarization approaches its limiting value. Here, the contribution of the f_2 eq. (28) is somewhat suppressed by the ratio of Yukawa couplings or the sbottom mixing angle. Note also that in the higgsino case, for certain values of the mixing angle, *e.g.* $\cos \theta_{\tilde{b}} = 0.5$, increasing the value of $\tan \beta$ can flip the sign of the polarization, this corresponds to the transition $\cos^2 \theta_{\tilde{b}} / \sin^2 \theta_{\tilde{b}} = h_b^2 / h_t^2$. Contours for the top polarization in the $\cos \theta_{\tilde{b}}$ vs $\tan \beta$ plane are displayed in Fig. 4 for both small and large values of Δm . In both cases any value of \mathcal{P}_t can be reached for any value of $\tan \beta$, although for $\Delta m = 10$ GeV and small $\tan \beta$ the polarization changes very rapidly with the sbottom mixing angle as a result of the kinematic factor f_2 in the denominator of eq. (28).

To see whether there is any hope to actually measure this polarization, we also need to

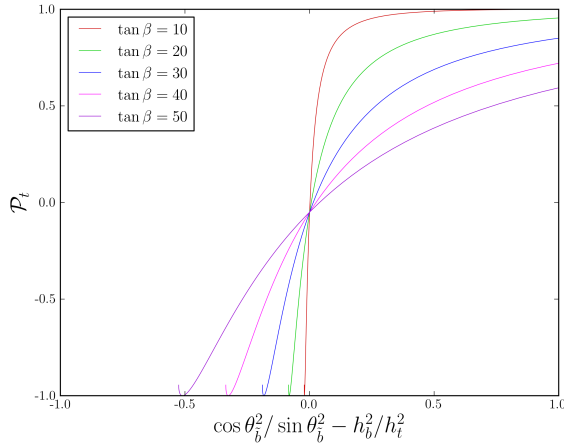


Figure 2: Dependence of the top polarization in $\tilde{b}_1 \rightarrow \tilde{\chi}_1^- t$ decays on the relative strength of the t and b Yukawa couplings and the sbottom mixing angle.

consider the sbottom production cross section and decay branching ratios. The branching ratios for \tilde{b}_1 decaying into charginos and neutralinos as function of the sbottom mixing angle are depicted in Fig. 5. The plot on the left shows the higgsino-like case. At small $\tan \beta$, the decay into $\tilde{\chi}_1^- t$ is always dominant even though the branching ratio is reduced when $\tilde{b}_1 \approx \tilde{b}_R$ ($\cos \theta_{\tilde{b}} \approx 0$), because the coupling strength of a \tilde{b}_R to a higgsino is proportional to the bottom Yukawa coupling. Therefore, at small $\cos \theta_{\tilde{b}}$, sbottom decays into charginos and each of the three lightest neutralinos become comparable (about 20–30%). For $\tan \beta = 50$, the bottom Yukawa coupling is large and the branching ratio to $\tilde{\chi}_1^- t$ is about 40–60% over the whole $\cos \theta_{\tilde{b}}$ range.

In the right panel of Fig. 5 the $\tilde{\chi}_1^-$ and $\tilde{\chi}_1^0$ are wino-like, $\tilde{\chi}_2^0$ is bino-like and $\tilde{\chi}_3^0, \tilde{\chi}_4^0$ are higgsino-like. The wino states do not couple to \tilde{b}_R , so for $\cos \theta_{\tilde{b}} \approx 0$ the decay $\tilde{b}_1 \rightarrow \tilde{\chi}_2^0 b$ dominates. As the \tilde{b}_L admixture increases, the branching ratio into the wino-like chargino increases because the coupling is proportional to top Yukawa coupling. The $\text{BR}(\tilde{b}_L \rightarrow \tilde{\chi}_1^- t)$ saturates at around 60% because it has to compete with the $\tilde{b}_L \rightarrow \tilde{\chi}_1^0 b$ decay, which has a BR around 40%.

The cross sections for sbottom (and stop) pair-production as a function of the sbottom (stop) mass, calculated at NLO at $\sqrt{s} = 14$ TeV with Prospino [33], are shown in Fig. 6. The processes $pp \rightarrow \tilde{b}_i \tilde{b}_i^*$, and likewise $t_i \tilde{t}_i^*$, ($i = 1, 2$) proceed through pure QCD interaction, the mixing angle in the stop or the sbottom sector enters the cross section calculations only through $\mathcal{O}(\alpha_s)$ corrections involving $t\tilde{t}\tilde{g}$ and the four-squark couplings. Thus the cross section for stop-pair production is very similar to that of sbottom-pair production. Mixed pairs $\tilde{t}_1 \tilde{t}_2$ and $\tilde{b}_1 \tilde{b}_2$ cannot be produced at lowest order since the $g\tilde{t}\tilde{t}$ and $g\tilde{g}\tilde{t}\tilde{t}$ vertices are diagonal in the chiral as well as in the mass basis. $\tilde{t}_i \tilde{b}_i$ production cross sections are suppressed by at least 2 orders of magnitude as compared to $\tilde{t}_i \tilde{t}_i$ and $\tilde{b}_i \tilde{b}_i$ productions, we ignore this production mode for stop and sbottom. The production cross section changes rapidly in the interesting mass range between 500 GeV and 1 TeV. For masses around 650 GeV, as considered in the benchmark scenarios below, we find a cross section of about 150 fb, which quickly falls off to

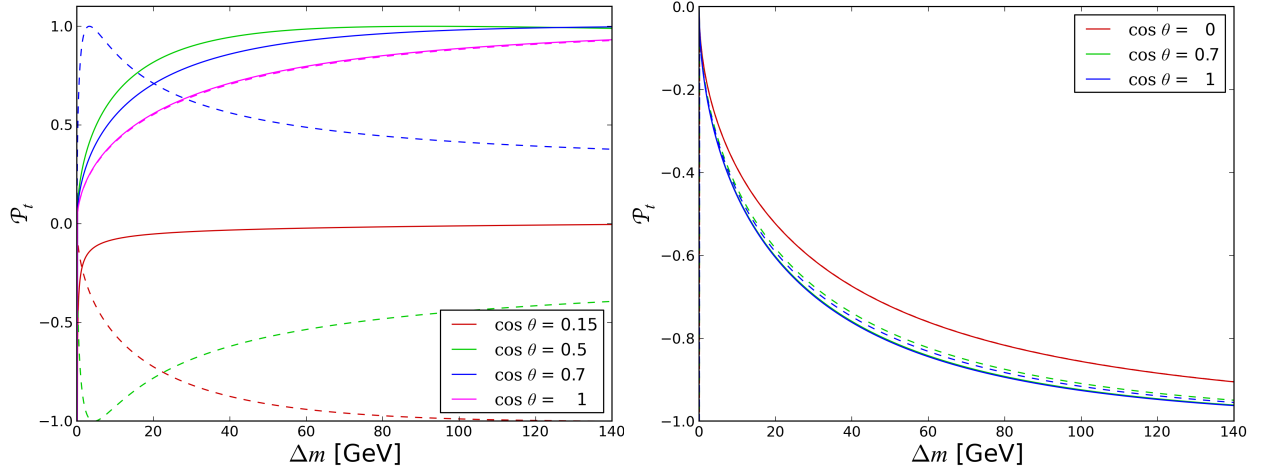


Figure 3: Top polarization in $\tilde{b}_1 \rightarrow \tilde{\chi}_1^- t$ decays as a function of $\Delta m \equiv m_{\tilde{b}_1} - m_{\tilde{\chi}_1^-} - m_t$ for various choices of $\cos \theta_{\tilde{b}}$; on the left for $\mu = 350$ GeV and $M_2 = 1000$ GeV (higgsino case), on the right for $M_2 = 350$ GeV and $\mu = 1000$ GeV (wino case). Solid lines represent $\tan \beta = 10$ and dashed lines are for $\tan \beta = 50$.

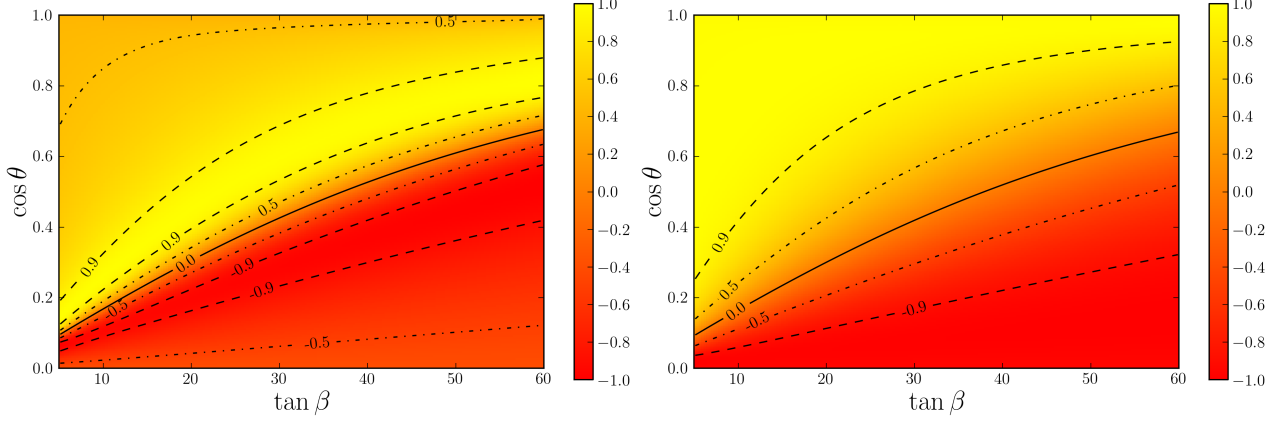


Figure 4: Contours of top polarization in the $\cos \theta$ versus $\tan \beta$ plane for the higgsino case with $\mu = 350$ GeV and $M_2 = 1000$ GeV, for a fixed mass difference of $\Delta m = 10$ GeV (left) and $\Delta m = 200$ GeV (right).

below 50 fb for around 800 GeV, see the small inset in Fig. 6.

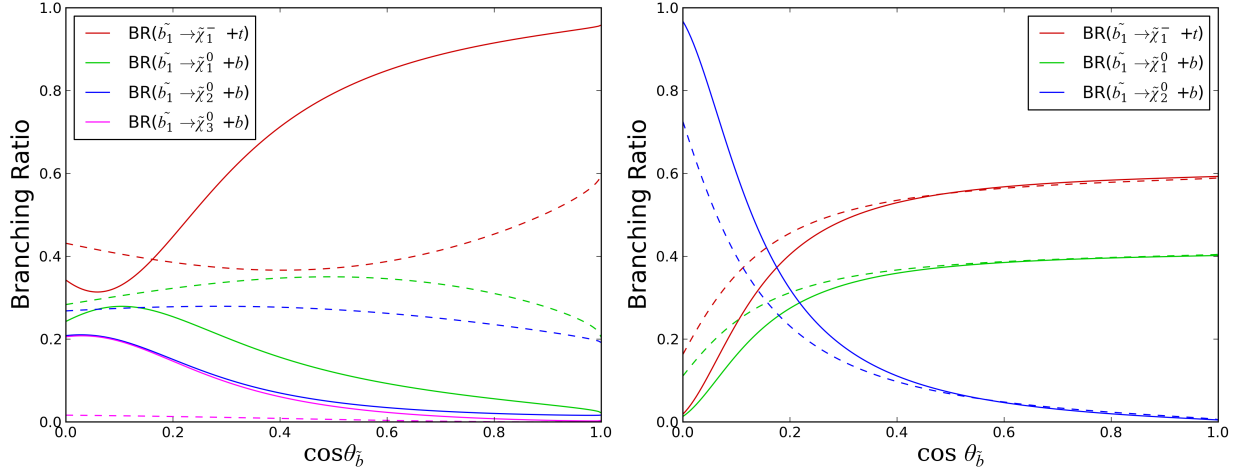


Figure 5: Branching ratios of \tilde{b}_1 as a function of $\cos \theta_{\tilde{b}}$ for $m_{\tilde{b}_1} = 685$ GeV, on the left for the higgsino case with $\mu = 350$ GeV and $M_2 = 1000$ GeV, on the right for the wino case with $\mu = 1000$ GeV and $M_2 = 350$ GeV. The solid (dashed) lines represent $\tan \beta = 10$ (50). The remaining parameters are as for benchmark point **bm-2** in Table 1.

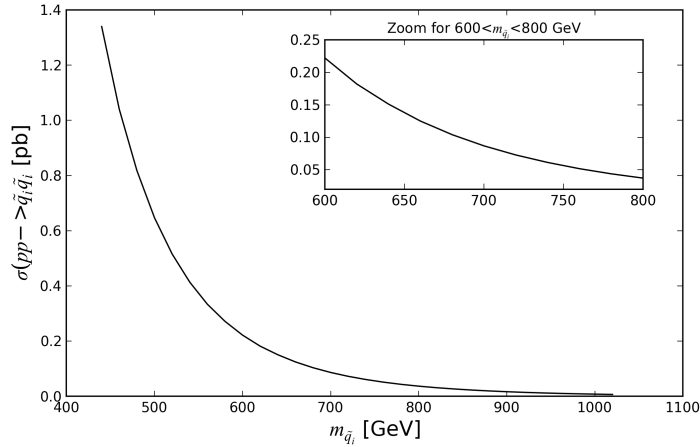


Figure 6: Stop and sbottom pair production cross sections at the LHC with $\sqrt{s} = 14$ TeV, computed at NLO with **Prospino**.

6.2 Benchmark scenarios

In a complete MSSM scenario, tops can also come from decays of stops, $\tilde{t}_{1,2}$, and of the heavier sbottom, \tilde{b}_2 . Some of these decays can be distinguished by their different signatures, for instance $\tilde{b}_1 \rightarrow t \tilde{\chi}_1^- \rightarrow tW \tilde{\chi}_1^0$ versus $\tilde{t}_1 \rightarrow t \tilde{\chi}_2^0 \rightarrow tZ \tilde{\chi}_1^0$ or $\tilde{t}_1 \rightarrow t \tilde{\chi}_1^0$. Others, like \tilde{b}_1 and \tilde{b}_2 both decaying to $t \tilde{\chi}_1^-$ give identical signatures. It is hence necessary to consistently add up the polarizations resulting from all processes which cannot be distinguished in the experimental analysis. In particular, if the masses of the $\tilde{\chi}_1^\pm$, $\tilde{\chi}_2^0$ and $\tilde{\chi}_1^0$ are close to each other, as is typically the case in higgsino or wino LSP scenarios, the $\tilde{\chi}_1^\pm$ and $\tilde{\chi}_2^0$ decays into the LSP will lead to soft decay products which are likely to be missed. In such a case, the processes

$$\begin{aligned}
 pp &\rightarrow \tilde{b}_1 \tilde{b}_1^*, & \tilde{b}_1 &\rightarrow t \tilde{\chi}_1^- \\
 pp &\rightarrow \tilde{b}_2 \tilde{b}_2^*, & \tilde{b}_2 &\rightarrow t \tilde{\chi}_1^- \\
 pp &\rightarrow \tilde{t}_1 \tilde{t}_1^*, & \tilde{t}_1 &\rightarrow t \tilde{\chi}_{1,2}^0
 \end{aligned}
 \tag{44}$$

may all contribute to the $t\bar{t} + E_T^{\text{miss}}$ signature, and the total or “net” top polarization relevant for the experimental analysis will be a result of the stop and sbottom production cross sections, their decay branching ratios and the relevant boosts for going from the rest frame to the lab frame. (We neglect the \tilde{t}_2 in eq. (44) because, in order to achieve $m_h \approx 126$ GeV, at least one of the stops should be heavy and will thus have a very low production cross section.)

In this context, we remind the reader that the situation of only \tilde{b}_1 being light and all other 3rd generation squarks heavy only occurs for $\tilde{b}_1 \sim \tilde{b}_R$. For $\tilde{b}_1 \sim \tilde{b}_L$, also the \tilde{t}_1 will be close in mass (or even lighter because of L–R mixing), because both their masses are governed by the same mass parameter $M_{\tilde{Q}_3}$.

For illustration and to allow a complete analysis, we present in Table 1 a set of 7 benchmark points which exemplify different scenarios of stop/sbotttom mass and mixing patterns and resulting top polarizations. The production cross sections, branching ratios and top polarizations \mathcal{P}_t originating from different decay processes in the respective squark rest frame are listed in Table 2. Moreover, Table 2 gives the net polarization $\hat{\mathcal{P}}_t$ in the laboratory frame, together with the values for the polar angle and azimuthal angle asymmetries defined in eqs. (35) and (36), summing over all processes that cannot be distinguished from $\tilde{b}_1 \rightarrow t \tilde{\chi}_1^-$.⁴

Since the dependence of the top polarization on the sbottom and stop masses and mixings is most interesting for the higgsino scenario, most of our examples focus on this case. Concretely, points **bm-1** to **bm-4** and **bm-6** have $\mu = 350$ GeV and $M_2 = 2M_1 = 1000$ GeV, as used earlier in this paper, leading to a 97% higgsino LSP and a $\tilde{\chi}_1^\pm - \tilde{\chi}_1^0$ mass difference of about 9 GeV; **bm-5** has a similar electroweak-ino pattern but for a lighter mass scale. The case of $\tilde{\chi}_1^\pm \sim \tilde{W}^\pm$ is exemplified in **bm-7**. For all points, the parameters in the squark sector are adjusted such that $m_{\tilde{b}_1} \approx 650$ GeV (to avoid kinematic effects on \mathcal{P}_t) and $m_h \approx 126$ GeV. All our benchmark points are for $\tan \beta = 10$; we do not present specific points for large $\tan \beta$ because they would not add any new features w.r.t. points **bm-1** to **bm-7**. Note also that we have chosen our benchmark points such that they lie (just) outside the current exclusion limits—prospects should be good

⁴Of course dedicated simulations would be necessary to decide whether or not specific processes can be distinguished. This is however beyond the scope of this paper. Instead we generally treat $\tilde{b}_1 \rightarrow t \tilde{\chi}_1^-$ and $\tilde{t}_1 \rightarrow t \tilde{\chi}_{1,2}^0$ as indistinguishable if the $\tilde{\chi}_1^\pm - \tilde{\chi}_1^0$ mass difference is small, below about 20 GeV.

	bm-1	bm-2	bm-3	bm-4	bm-5	bm-6	bm-7
$M_{\tilde{Q}_3}$	571	1300	630	610	582	850	600
$M_{\tilde{D}_3}$	1500	572	597	599	1500	601.5	609
$M_{\tilde{U}_3}$	2200	1300	2200	2200	2200	1500	2200
M_1	500	500	500	500	200	500	250
M_2	1000	1000	1000	1000	400	1000	350
μ	350	350	350	350	150	350	1000
$m_{\tilde{b}_1}$	650.41	650.44	650.85	650.13	650.08	650.17	650.71
$m_{\tilde{b}_2}$	1537.39	1329.77	707.36	688.72	1538.10	884.47	692.45
$\cos\theta_{\tilde{b}}$	0.999	0.006	0.10	0.15	0.999	0.02	0.42
$m_{\tilde{t}_1}$	630.18	1236.20	687.92	668.37	633.84	818.99	667.61
$m_{\tilde{t}_2}$	2210.95	1560.58	2208.66	2209.42	2212.19	1518.19	2205.97
$\cos\theta_{\tilde{t}}$	0.995	0.85	0.995	0.995	0.996	0.96	0.996
$m_{\tilde{\chi}_1^-}$	351.91	352.73	352.04	351.98	144.16	352.05	360.35
$m_{\tilde{\chi}_2^-}$	1013.41	1021.05	1013.45	1013.42	430.32	1016.09	1008.07
$m_{\tilde{\chi}_1^0}$	343.06	343.39	343.10	343.08	126.52	343.13	247.08
$m_{\tilde{\chi}_2^0}$	357.41	358.22	357.58	357.50	159.18	357.22	360.10
$m_{\tilde{\chi}_3^0}$	502.99	500.89	502.32	502.45	213.20	502.61	1002.10
$m_{\tilde{\chi}_4^0}$	1013.95	1021.33	1014.02	1013.98	431.95	1016.63	1008.24
$\text{BR}_{B \rightarrow X_s \gamma}$	3.53	3.61	3.51	3.51	3.26	3.78	3.31
$\text{BR}_{B_s \rightarrow \mu^+ \mu^-}$	3.04	3.04	3.03	3.04	3.04	3.03	3.03

Table 1: Parameters and masses (in GeV) for seven illustrative benchmark points. All points have $\tan\beta = 10$ and $A_b = 100$ GeV, while $A_t \approx 3$ TeV is adjusted such that $m_h \approx 126$ GeV. The values for $\text{BR}(B \rightarrow X_s \gamma)$ and $\text{BR}(B_s \rightarrow \mu^+ \mu^-)$ are given in units of 10^{-4} and 10^{-9} , respectively.

to test them early in the next phase of LHC running at 13–14 TeV. The detailed characteristics of the various benchmark points are as follows:

- **bm-1** features a higgsino scenario with an almost pure LH \tilde{b}_1 , for which we expect a top polarization in $\tilde{b}_1 \rightarrow t \tilde{\chi}_1^-$ decays ($\text{BR} \sim 96\%$) close to +1. As the light sbottom mass is determined by $M_{\tilde{Q}_3} = 571$ GeV, also the \tilde{t}_1 is light; in fact it is 20 GeV lighter than the \tilde{b}_1 and decays with 96% BR to $t \tilde{\chi}_{1,2}^0$, thus adding to the signal and the net polarization of interest. The \tilde{b}_2 and \tilde{t}_2 are heavy and play no role for our analysis. The tops stemming from \tilde{t}_1 decays also have a polarization close to +1, so we expect a large positive net polarization, diluted only by boost effects. Indeed, we find $\hat{P}_t = 0.75$ for this scenario, together with rather large asymmetries $A_{\theta_t} \approx 0.6$ and $A_{\phi_t} \approx 0.8$.
- **bm-2** is an example of the higgsino scenario with an almost pure RH \tilde{b}_1 , leading to a top polarization close to -1 in $\tilde{b}_1 \rightarrow t \tilde{\chi}_1^-$ decays. The \tilde{t}_1 can be chosen heavy in this case, so that the only relevant cross section is $\tilde{b}_1 \tilde{b}_1^*$ production. Compared to **bm-1**, the total signal is further reduced by the smaller $\text{BR}(\tilde{b}_1 \rightarrow t \tilde{\chi}_1^-)$ of only 34%. In the lab frame, we

	bm-1	bm-2	bm-3	bm-4	bm-5	bm-6	bm-7
$\sigma(pp \rightarrow \tilde{b}_1 \tilde{b}_1^*)$ [pb]	0.137	0.137	0.137	0.137	0.137	0.137	0.137
$\sigma(pp \rightarrow \tilde{b}_2 \tilde{b}_2^*)$ [pb]	$< 10^{-3}$	0.001	0.082	0.096	$< 10^{-3}$	0.019	0.093
$\sigma(pp \rightarrow \tilde{t}_1 \tilde{t}_1^*)$ [pb]	0.163	0.002	0.095	0.114	0.157	0.033	0.115
$\text{BR}(\tilde{b}_1 \rightarrow t \tilde{\chi}_1^-)$	0.96	0.34	0.31	0.35	0.72	0.32	0.41
$\text{BR}(\tilde{b}_1 \rightarrow t \tilde{\chi}_2^-)$	–	–	–	–	0.16	–	–
$\text{BR}(\tilde{b}_2 \rightarrow t \tilde{\chi}_1^-)$	0.30	0.82	0.96	0.96	0.29	0.96	0.58
$\text{BR}(\tilde{b}_2 \rightarrow t \tilde{\chi}_2^-)$	$< 10^{-3}$	0.09	–	–	0.01	–	–
$\text{BR}(\tilde{t}_1 \rightarrow t \tilde{\chi}_1^0)$	0.51	0.33	0.50	0.50	0.27	0.47	0.01
$\text{BR}(\tilde{t}_1 \rightarrow t \tilde{\chi}_2^0)$	0.45	0.35	0.47	0.46	0.40	0.42	0.26
$\mathcal{P}_t(\tilde{b}_1 \rightarrow t \tilde{\chi}_1^-)$	0.92	–0.92	–0.56	–0.05	0.99	–0.98	–0.94
$\mathcal{P}_t(\tilde{b}_1 \rightarrow t \tilde{\chi}_2^-)$	–	–	–	–	–0.29	–	–
$\mathcal{P}_t(\tilde{b}_2 \rightarrow t \tilde{\chi}_1^-)$	–0.99	0.99	0.95	0.94	–0.99	0.99	–0.97
$\mathcal{P}_t(\tilde{b}_2 \rightarrow t \tilde{\chi}_2^-)$	–0.94	–0.67	–	–	–0.99	–	–
$\mathcal{P}_t(\tilde{t}_1 \rightarrow t \tilde{\chi}_1^0)$	0.82	0.40	0.88	0.86	0.99	0.94	–0.99
$\mathcal{P}_t(\tilde{t}_1 \rightarrow t \tilde{\chi}_2^0)$	0.92	0.50	0.97	0.96	0.99	0.99	–0.95
$\widehat{\mathcal{P}}_t$ (total)	0.75	–0.73	0.46	0.64	0.92	0.07	–0.83
A_{θ_t}	0.59	0.14	0.61	0.60	0.80	0.47	0.12
A_{ϕ_t}	0.84	0.57	0.83	0.84	0.92	0.76	0.55

Table 2: Production cross sections at $\sqrt{s} = 14$ TeV, decay branching ratios, top polarizations originating from different decay processes in the respective squark rest frame, total polarization in the laboratory frame, as well as polar and azimuthal angle asymmetries for the benchmark points defined in Table 1.

have $\widehat{\mathcal{P}}_t = -0.73$ for this scenario, with a small polar angle asymmetry of $A_{\theta_t} \approx 0.1$ but a still sizable azimuthal angle asymmetry of $A_{\phi_t} \approx 0.6$.

- **bm-3** and **bm-4** illustrate the case of intermediate polarization, which is achieved by giving the mostly RH \tilde{b}_1 a small \tilde{b}_L component. Point **bm-3** has $\cos \theta_{\tilde{b}} = 0.1$ and $\mathcal{P}_t(\tilde{b}_1 \rightarrow t \tilde{\chi}_1^-) = -0.5$, while **bm-4** has $\cos \theta_{\tilde{b}} = 0.15$ and $\mathcal{P}_t(\tilde{b}_1 \rightarrow t \tilde{\chi}_1^-) \approx 0$. In contrast to the two previous points, both \tilde{b}_2 and \tilde{t}_1 have masses around 700 GeV (*i.e.* not far from the \tilde{b}_1) and thus also significantly contribute, in particular because both $\text{BR}(\tilde{b}_2 \rightarrow t \tilde{\chi}_1^-)$ and $\text{BR}(\tilde{t}_1 \rightarrow t \tilde{\chi}_{1,2}^0)$ are very large, around 96%. The net polarization in the lab frame turns out to be 0.46 (0.64) for **bm-3** (**bm-4**). The polar and azimuthal angle asymmetries are sizable, $A_{\theta_t} \approx 0.6$ and $A_{\phi_t} \approx 0.8$, for both points. Note however that with roughly 210–250 fb the total rate ($\sigma \times \text{BR}$'s) before cuts for $t\bar{t} + E_T^{\text{miss}}$ is smaller than for **bm-1** (roughly 290 fb).
- **bm-5** is an example for the situation when both charginos are light enough to allow $\tilde{b}_1 \rightarrow t \tilde{\chi}_1^-$ and $\tilde{b}_1 \rightarrow t \tilde{\chi}_2^-$ decays. As before, the LSP is mostly higgsino and the $\tilde{\chi}_1^\pm - \tilde{\chi}_1^0$ mass difference is small, such that the $\tilde{\chi}_1^\pm \rightarrow \tilde{\chi}_1^0 W^*$ is probably missed. The $\tilde{\chi}_2^\pm$ on the other hand is wino-like and decays to $\tilde{\chi}_1^0$ plus an on-shell W . The top polarization in the sbottom rest frame is $\approx +1$ for \tilde{b}_1 decays into $t \tilde{\chi}_1^-$, while it has a small negative

value, $\mathcal{P}_t = -0.29$, for the decays into $t\tilde{\chi}_2^-$. As for **bm-1**, the \tilde{t}_1 is also light and decays with $\sim 67\%$ to $t\tilde{\chi}_{1,2}^0$. The top polarization in these decays, which can likely not be distinguished from $\tilde{b}_1 \rightarrow t\tilde{\chi}_1^-$, is close to $+1$. We end up with $\hat{\mathcal{P}}_t = +0.92$ in the lab frame and large asymmetries of $A_{\theta_l} \approx 0.8$ and $A_{\phi_l} \approx 0.9$.

- **bm-6** is a variant of **bm-3** with somewhat heavier \tilde{t}_1 and \tilde{b}_2 . It is constructed such that the net polarization resulting from the combination of $\mathcal{P}_t(\tilde{b}_1 \rightarrow t\tilde{\chi}_1^-) \approx +1$ and $\mathcal{P}_t(\tilde{t}_1 \rightarrow t\tilde{\chi}_{1,2}^0) \approx -1$ is almost zero. Nonetheless the asymmetry parameters are sizable, $A_{\theta_l} \approx 0.5$ and $A_{\phi_l} \approx 0.8$.
- **bm-7** shows the wino-like $\tilde{\chi}_1^\pm$ case, which gives $\mathcal{P}_t \approx -1$ in sbottom decays whatever is the sbottom mixing angle. Note that the \tilde{t}_1 decays into $t\tilde{\chi}_1^0$ or $t\tilde{\chi}_2^0$ also give $\mathcal{P}_t \approx -1$. However, these decays can in principle be distinguished, as $m_{\tilde{\chi}_1^0} \simeq 250$ GeV and $\tilde{\chi}_2^0 \rightarrow Z\tilde{\chi}_1^0$ and $\tilde{\chi}_1^\pm \rightarrow W\tilde{\chi}_1^0$. To estimate $\hat{\mathcal{P}}_t$ and the leptonic asymmetries, we sum over \tilde{b}_1 and \tilde{b}_2 production followed by decays into $t\tilde{\chi}_1^\pm$. We find $\hat{\mathcal{P}}_t = -0.83$, $A_{\theta_l} \approx 0.1$ and $A_{\phi_l} \approx 0.5$.

6.3 Polarization dependent kinematic distributions

In this section we present results for the polarization-dependent kinematic distributions of the top decay products introduced in Section 4. As mentioned, these distributions depend on the top polarization in the sfermion rest frame, the top boost in the laboratory frame and the transverse momentum of the top quark. As a result they are influenced by the mass difference between the decaying sfermion and the daughter electroweak-ino as discussed in ref. [22]. Here, we concentrate on the case of large mass difference. More concretely, we analyze the lepton energy distributions as well as the energy ratios z and u of eq. (37) for **bm-2**, **bm-5** and **bm-6**, corresponding to close to ± 1 and zero net polarization, respectively.

Figure 7 shows the lepton energy E_l (left) and transverse momentum p_T^l (right) distributions for **bm-2**, **bm-5** and **bm-6**. As can be seen from eq. (33) for a positively polarized top, the decay leptons go preferentially in the forward direction and hence, including the boost, the energy and transverse momentum of the leptons are larger than in the unpolarized or negatively polarized case. For the negatively polarized top, the situation is opposite, the leptons gain less energy and the distributions peak at smaller values. This effect is clearly seen in both the E_l and p_T^l distributions in Fig. 7 when comparing the lines for $\mathcal{P}_t = +0.92$, 0.07 and -0.73 .

We conclude that for $\tilde{b}_1 \sim \tilde{b}_L$ decaying into a higgsino-like chargino (and/or $\tilde{t}_1 \sim \tilde{t}_L$ decaying into top+neutralino [22]), the harder E_l and p_T^l distributions can be used to extend the reach of searches for 3rd generation squarks. On the other hand, for scenarios which lead to small or negative top polarization, the opposite conclusion holds. Note, however, that the polarization-dependence of the E_l and p_T^l distributions makes a general interpretation in terms of SMS [36,37] difficult if information on the polarization is used in the analysis.

The behavior of the E_l and p_T^l distributions for different polarizations seen in Fig. 7 is a reflection of the angular distribution of the lepton w.r.t. the top quark spin direction in the rest frame given by eq. (33). Since κ_l and κ_b have opposite signs, the corresponding distributions for b -jets will show the opposite behavior. Figure 8 shows the b -jet energy E^b (left) and transverse

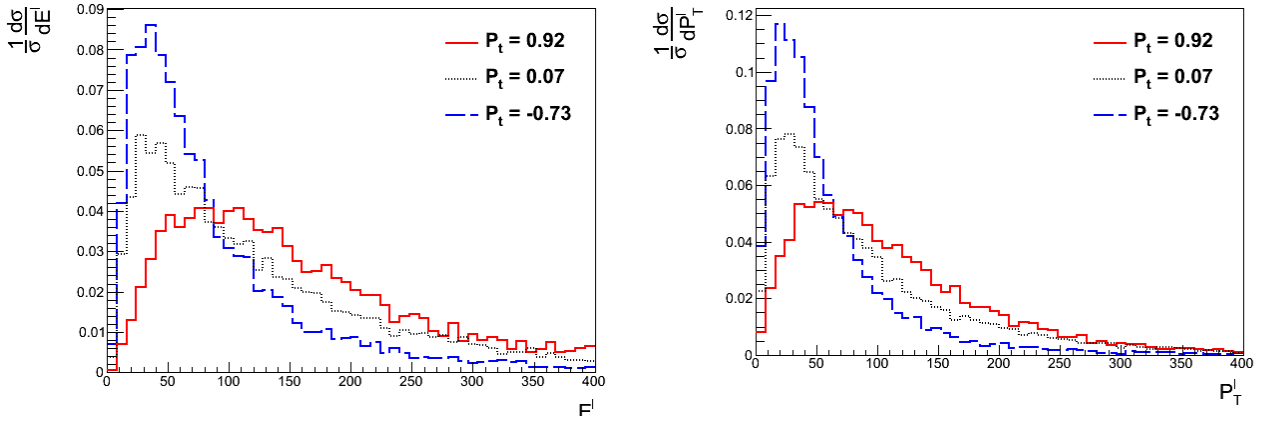


Figure 7: Lepton energy E_l (left) and transverse momentum p_T^l (right) distributions for three different polarizations. The dashed blue lines are for **bm-2** with $\widehat{P}_t = -0.73$, the full red lines are for **bm-5** with $\widehat{P}_t = 0.92$, and the dotted black lines are for **bm-6** with $\widehat{P}_t = 0.07$.

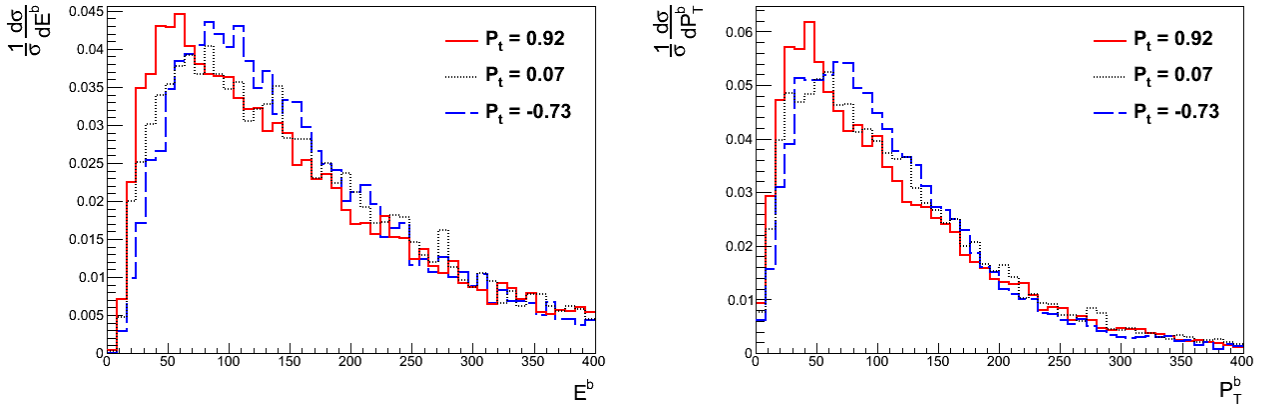


Figure 8: Same as Fig. 7 but for b -jet energy E^b (left) and transverse momentum p_T^b (right) distributions.

momentum p_T^b (right) distributions for **bm-2**, **bm-5** and **bm-6**. Although the size of the effect is smaller than for leptons due to the smaller value of κ_b , the b -jet distributions may still provide interesting complementary information. In particular, the distributions get harder as the top polarization changes from $+1$ to -1 . Thus the loss of reach due to a softened lepton spectrum in case of a negatively polarized top might be compensated to some extent by the harder b -jet spectrum.

In Section 4 we also discussed that the azimuthal angle asymmetry A_{ϕ_l} and the polar angle asymmetry A_{θ_l} may also give us a quantitative measure for the top polarization. To illustrate this point, we show in Fig. 9 the azimuthal angle ϕ_l (left) and polar angle θ_l (right) distributions of the decay leptons for **bm-2**, **bm-5** and **bm-6**. As expected, the distributions for ϕ_l peak at

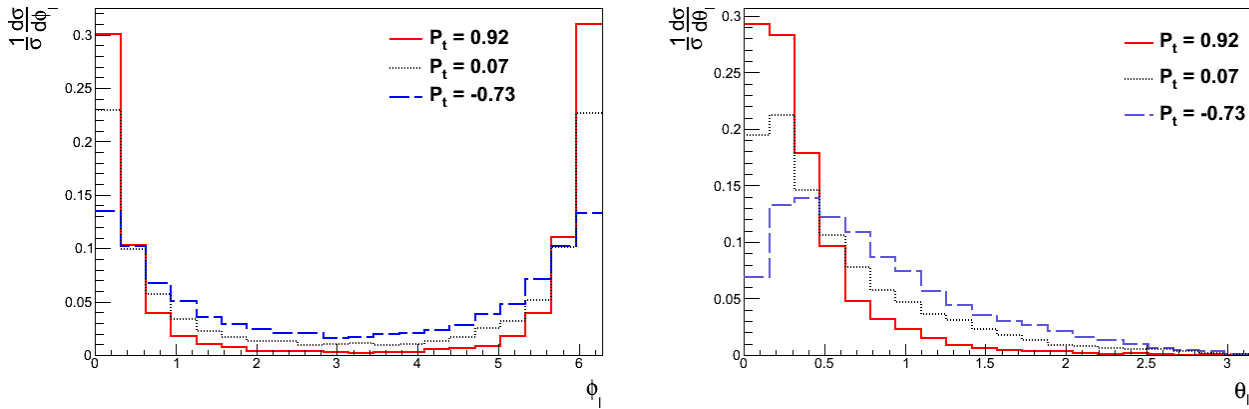


Figure 9: Distributions of the azimuthal angle ϕ_l (left) and the polar angle θ_l (right) of the decay lepton. The dashed blue lines are for **bm-2** with $\widehat{\mathcal{P}}_t = -0.73$, the full red lines are for **bm-5** with $\widehat{\mathcal{P}}_t = 0.92$, and the dotted black lines are for **bm-6** with $\widehat{\mathcal{P}}_t = 0.07$.

$\phi_l = 0$ and $\phi_l = 2\pi$ for all the three cases, but the peaks are higher for a positively polarized tops as compared to unpolarized or the negatively polarized ones. A similar situation is seen for the distribution of the polar angle θ_l : the peaking is again in the direction of the top boost and increases when going from negative to positive polarization. The specific values of the asymmetries A_{θ_l} and A_{ϕ_l} , defined by eqs. (35) and (36), are given in Table 2. The values of both the asymmetries are the lowest for negative polarization and increase as the polarization goes to 1, thus making them a measure of the polarization.

The above observables concerning angular distributions of the leptons are independent of the anomalous tbW coupling. At LHC-14, however, the tops will be highly boosted and it may not be easy to use the angular observables. The boost distribution of the tops for the three benchmark points under consideration is shown in Fig. 10. The boost is of course independent of the top polarization—the small differences in the boost distributions arise from the different stop and sbottom masses for the three benchmark scenarios. The main point is that the tops are typically highly boosted. In such a situation, the energy ratios u and z defined in eq. (37) may give very useful information. (Recall that these observables can be however affected by nonzero values of an anomalous tbW coupling.) A cut on the top boost β_t can enhance the dependence on the polarization.

Figure 11 shows the distributions of the energy ratio u for different cuts on β_t . The distributions are weighted towards smaller values of u for negatively polarized tops, and towards higher values of u for a positive polarization. The cut on the boost enhances the separation of +ve and -ve polarization. The analogous distributions of the energy ratio z are shown in Fig. 12. As expected from the discussion in Section 4, the behavior of z is opposite to that of u , that is positive polarization favours low z values. A cut on β_t again helps to better differentiate between different values of polarization. Clearly, asymmetries similar to A_{θ_l} and A_{ϕ_l} can be constructed for u and z and may serve as an additional measure of the polarization.

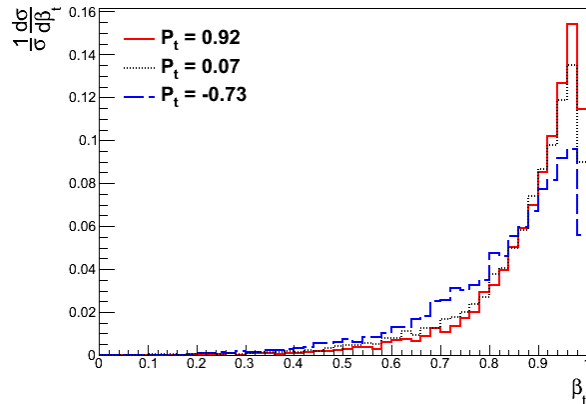


Figure 10: The top boost distribution at 14 TeV, for **bm-2** with $\widehat{P}_t = -0.73$ (dashed blue line), **bm-5** with $\widehat{P}_t = 0.92$ (full red line), and **bm-6** with $\widehat{P}_t = 0.07$ (dotted black line).

7 Conclusions

Given the increasingly strong limits on squark and gluino masses from searches at the LHC, together with a SM-like Higgs boson with $m_h \approx 125$ GeV, “natural SUSY” with light 3rd generation squarks, maximal stop mixing, and perhaps light higgsinos emerges as the new phenomenological paradigm for SUSY phenomenology to be addressed by the next phase of LHC running at 13–14 TeV. It is therefore particularly interesting and timely to develop methods to a) enhance the discovery potential for stops and sbottoms and b) determine their properties at the LHC.

In this paper we discussed the polarization of top quarks stemming from sbottom and stop decays as a useful tool to this end. In particular we investigated in detail the behavior of the top polarization in sbottom decays into charginos, $\tilde{b} \rightarrow t\tilde{\chi}^-$. As in the case of stop decays to $t\tilde{\chi}^0$, this polarization may give clues to the nature of both the sbottom and the chargino. Concretely, we pointed out that for a mostly wino-like chargino, the top polarization is always ≈ -1 , while for a higgsino-like chargino it can take any value between -1 and $+1$, depending on the sbottom mixing angle. Moreover, we discussed that in realistic setups the relation between top polarization and underlying MSSM scenario may not be straightforward because the tops may come from several different channels. For example, when the lighter sbottom \tilde{b}_1 has a large LH component, its mass is similar to that of the lighter stop \tilde{t}_1 (as both are determined by the same soft mass parameter), and therefore both stop and sbottom decays may lead to the same signature, and only the net polarization resulting from all different decays will be measurable.

We illustrated the relation between the top polarizations from specific decay channels (in the respective stop or sbottom rest frame) and the net polarization in the laboratory by means of seven benchmark points. Furthermore, we studied how the top polarization affects its decay kinematics and pointed out the strong correlation between the polarization of the top quark and the kinematical distributions of the various decay products. We observed how these may be used to enhance and evaluate the discovery reach, as well as to construct measures of this

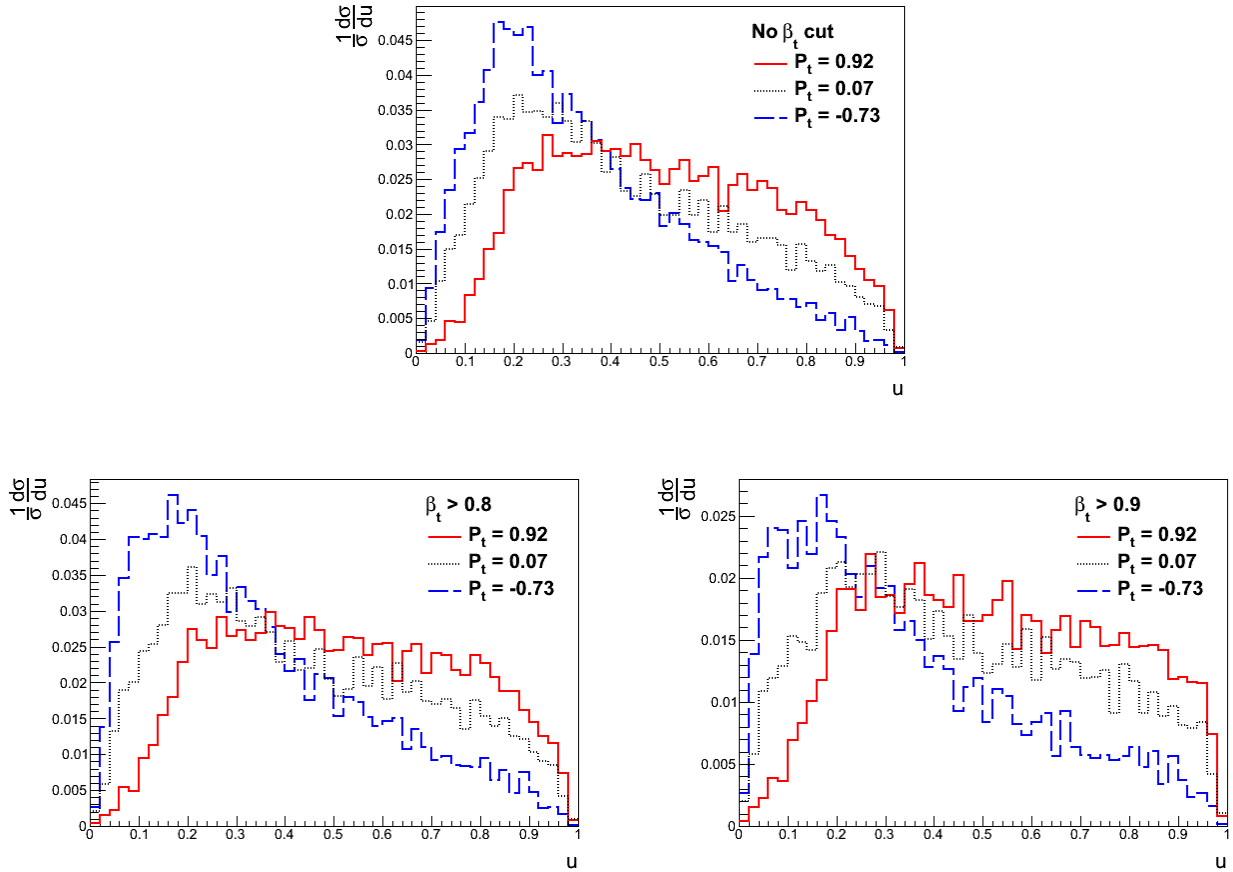


Figure 11: Distributions of the energy ratio u , without cut on the boost (top), for $\beta_t > 0.8$ (lower left) and for $\beta_t > 0.9$ (lower right). The dashed blue lines are for **bm-2** with $\hat{\mathcal{P}}_t = -0.73$, the full red lines are for **bm-5** with $\hat{\mathcal{P}}_t = 0.92$, and the dotted black lines are for **bm-6** with $\hat{\mathcal{P}}_t = 0.07$. The distributions show a strong dependence on the values of polarization considered.

polarization using the angular observables of the decay lepton.

In summary, we have shown that top polarization may provide a useful tool for the searches for 3rd generation squarks, in particular in the context of natural SUSY with light higgsinos, a scenario which is very difficult to resolve at the LHC.

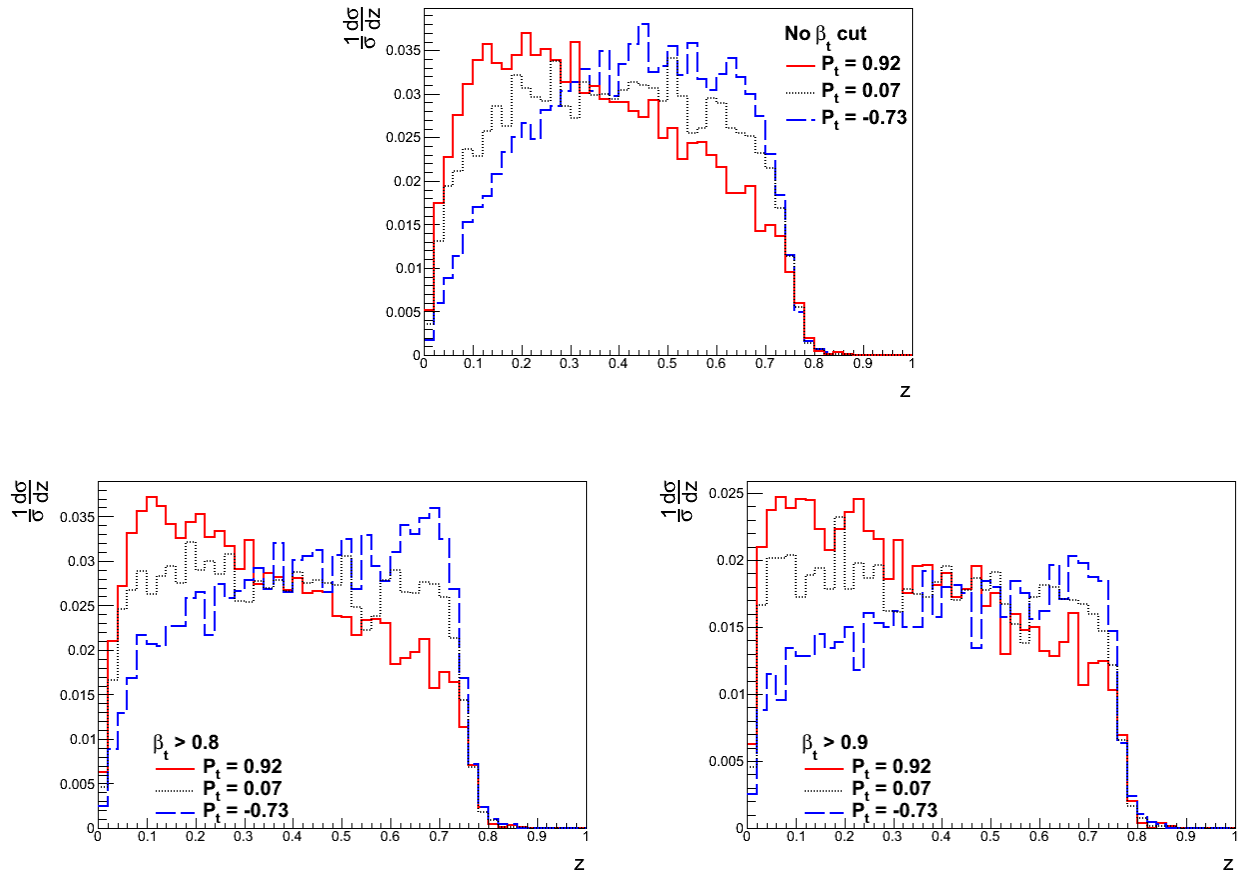


Figure 12: Distributions of the energy ratio z , without cut on the boost (top), for $\beta_t > 0.8$ (lower left) and for $\beta_t > 0.9$ (lower right). The dashed blue lines are for $\mathbf{bm-2}$ with $\widehat{\mathcal{P}}_t = -0.73$, the full red lines are for $\mathbf{bm-5}$ with $\widehat{\mathcal{P}}_t = 0.92$, and the dotted black lines are for $\mathbf{bm-}$ with $\widehat{\mathcal{P}}_t = 0.07$. The distributions show a strong dependence on the values of polarization considered.

Acknowledgements

We thank I. Niessen and A. Pukhov for help with technical questions and Dan Tovey for useful discussions. This work was partly funded by the French ANR project DMAstroLHC. GB and SK \times 2 also thank the Galileo Galilei Institute for Theoretical Physics (GGI Florence) for hospitality and the INFN for partial support. RG wishes to thank the theory group at LPSC (Grenoble) for hospitality when part of this work was done. In addition she would like to acknowledge support from the Department of Science and Technology, India under the J.C. Bose Fellowship scheme under grant no. SR/S2/JCB-64/2007.

References

- [1] **ATLAS** Collaboration, G. Aad et al., *Observation of a new particle in the search for the Standard Model Higgs boson with the ATLAS detector at the LHC*, *Phys.Lett.* **B716** (2012) 1–29, [[arXiv:1207.7214](#)].
- [2] **CMS** Collaboration, S. Chatrchyan et al., *Observation of a new boson at a mass of 125 GeV with the CMS experiment at the LHC*, *Phys.Lett.* **B716** (2012) 30–61, [[arXiv:1207.7235](#)].
- [3] **ATLAS** Collaboration, *Search for direct production of the top squark in the all-hadronic $t\bar{t} + E_{Tmiss}$ final state in 21 fb^{-1} of p - p collisions at $\sqrt{s} = 8 \text{ TeV}$ with the ATLAS detector*, March, 2013. presented at 48th Rencontres de Moriond on QCD and High Energy Interactions, La Thuile, March 2013, ATLAS-CONF-2013-024.
- [4] **ATLAS** Collaboration, *Search for direct stop production in events with missing transverse momentum and two b -jets using 12.8 fb^{-1} of pp collisions at $\sqrt{s} = 8 \text{ TeV}$ with the ATLAS detector*, Jan., 2013. ATLAS-CONF-2013-001.
- [5] **ATLAS** Collaboration, *Search for direct sbottom production in event with two b -jets using 12.8 fb^{-1} of pp collisions at $\sqrt{s} = 8 \text{ TeV}$ with the ATLAS Detector.*, Dec., 2012. ATLAS-CONF-2012-165.
- [6] R. Godbole, L. Hartgring, I. Niessen, and C. White, *Polarisation studies in H - t production*, [arXiv:1301.6877](#).
- [7] M. Jezabek and J. H. Kuhn, *Lepton Spectra from Heavy Quark Decay*, *Nucl.Phys.* **B320** (1989) 20.
- [8] A. Czarnecki, M. Jezabek, and J. H. Kuhn, *Lepton spectra from decays of polarized top quarks*, *Nucl.Phys.* **B351** (1991) 70–80.
- [9] A. Brandenburg, Z. Si, and P. Uwer, *QCD corrected spin analyzing power of jets in decays of polarized top quarks*, *Phys.Lett.* **B539** (2002) 235–241, [[hep-ph/0205023](#)].
- [10] B. Grzadkowski and Z. Hioki, *Angular distribution of leptons in general $t\bar{t}$ production and decay*, *Phys.Lett.* **B529** (2002) 82–86, [[hep-ph/0112361](#)].
- [11] B. Grzadkowski and Z. Hioki, *Decoupling of anomalous top decay vertices in angular distribution of secondary particles*, *Phys.Lett.* **B557** (2003) 55–59, [[hep-ph/0208079](#)].
- [12] R. M. Godbole, S. D. Rindani, and R. K. Singh, *Study of CP property of the Higgs at a photon collider using $\gamma\gamma \rightarrow t\bar{t} \rightarrow lX$* , *Phys.Rev.* **D67** (2003) 095009, [[hep-ph/0211136](#)].
- [13] R. M. Godbole, S. D. Rindani, and R. K. Singh, *Lepton distribution as a probe of new physics in production and decay of the t quark and its polarization*, *JHEP* **0612** (2006) 021, [[hep-ph/0605100](#)].

- [14] R. M. Godbole, K. Rao, S. D. Rindani, and R. K. Singh, *On measurement of top polarization as a probe of $t\bar{t}$ production mechanisms at the LHC*, *JHEP* **1011** (2010) 144, [[arXiv:1010.1458](#)].
- [15] E. L. Berger, Q.-H. Cao, J.-H. Yu, and H. Zhang, *Measuring Top Quark Polarization in Top Pair plus Missing Energy Events*, *Phys.Rev.Lett.* **109** (2012) 152004, [[arXiv:1207.1101](#)].
- [16] D. Krohn, J. Shelton, and L.-T. Wang, *Measuring the Polarization of Boosted Hadronic Tops*, *JHEP* **1007** (2010) 041, [[arXiv:0909.3855](#)].
- [17] **ATLAS** Collaboration, *Measurement of top quark polarisation in $t\bar{t}$ events with the ATLAS detector in proton-proton collisions at $\sqrt{s} = 7\text{TeV}$.*, Sep., 2012. ATLAS-CONF-2012-133.
- [18] E. Boos, H. Martyn, G. A. Moortgat-Pick, M. Sachwitz, A. Sherstnev, et al., *Polarization in sfermion decays: Determining $\tan\beta$ and trilinear couplings*, *Eur.Phys.J.* **C30** (2003) 395–407, [[hep-ph/0303110](#)].
- [19] T. Gajdosik, R. M. Godbole, and S. Kraml, *Fermion polarization in sfermion decays as a probe of CP phases in the MSSM*, *JHEP* **0409** (2004) 051, [[hep-ph/0405167](#)].
- [20] M. Perelstein and A. Weiler, *Polarized Tops from Stop Decays at the LHC*, *JHEP* **0903** (2009) 141, [[arXiv:0811.1024](#)].
- [21] B. Bhattacherjee, S. K. Mandal, and M. Nojiri, *Top Polarization and Stop Mixing from Boosted Jet Substructure*, [arXiv:1211.7261](#).
- [22] G. Bélanger, R. Godbole, L. Hartgring, and I. Niessen, *Top Polarization in Stop Production at the LHC*, [arXiv:1212.3526](#).
- [23] I. Low, *Polarized Charginos (and Tops) in Stop Decays*, [arXiv:1304.0491](#).
- [24] **CMS** Collaboration, *Search for direct top squark pair production in events with a single isolated lepton, jets and missing transverse energy at $s = 8\text{TeV}$ at $\sqrt{s} = 8\text{TeV}$* , Dec., 2012. CMS-PAS-SUS-12-023.
- [25] B. Hooberman, *Search for top and bottom squarks at CMS*, Nov., 2012. presented at HCP2012, Kyoto, Japan, https://twiki.cern.ch/twiki/pub/CMSPublic/PhysicsResultsSUS12023/CMS_ATLAS_comparison.pdf.
- [26] R. M. Godbole, L. Hartgring, I. Niessen, and C. D. White, *Top polarisation studies in H^-t and Wt production*, *JHEP* **1201** (2012) 011, [[arXiv:1111.0759](#)].
- [27] W. Bernreuther, *Top quark physics at the LHC*, *J.Phys.* **G35** (2008) 083001, [[arXiv:0805.1333](#)].
- [28] L. G. Almeida, S. J. Lee, G. Perez, I. Sung, and J. Virzi, *Top Jets at the LHC*, *Phys.Rev.* **D79** (2009) 074012, [[arXiv:0810.0934](#)].

- [29] J. Shelton, *Polarized tops from new physics: signals and observables*, *Phys.Rev.* **D79** (2009) 014032, [[arXiv:0811.0569](#)].
- [30] B. Allanach, *SOFTSUSY: a program for calculating supersymmetric spectra*, *Comput.Phys.Commun.* **143** (2002) 305–331, [[hep-ph/0104145](#)].
- [31] G. Bélanger, F. Boudjema, A. Pukhov, and A. Semenov, *micrOMEGAs: Version 1.3*, *Comput.Phys.Commun.* **174** (2006) 577–604, [[hep-ph/0405253](#)].
- [32] G. Bélanger, F. Boudjema, P. Brun, A. Pukhov, S. Rosier-Lees, et al., *Indirect search for dark matter with micrOMEGAs2.4*, *Comput.Phys.Commun.* **182** (2011) 842–856, [[arXiv:1004.1092](#)].
- [33] W. Beenakker, R. Hopker, and M. Spira, *PROSPINO: A Program for the production of supersymmetric particles in next-to-leading order QCD*, [hep-ph/9611232](#).
- [34] J. Alwall, P. Demin, S. de Visscher, R. Frederix, M. Herquet, et al., *MadGraph/MadEvent v4: The New Web Generation*, *JHEP* **0709** (2007) 028, [[arXiv:0706.2334](#)].
- [35] J. Alwall, M. Herquet, F. Maltoni, O. Mattelaer, and T. Stelzer, *MadGraph 5 : Going Beyond*, *JHEP* **1106** (2011) 128, [[arXiv:1106.0522](#)].
- [36] **ATLAS** Collaboration, H. Okawa and f. t. A. Collaboration, *Interpretations of SUSY Searches in ATLAS with Simplified Models*, [arXiv:1110.0282](#).
- [37] **CMS** Collaboration, S. Chatrchyan et al., *Interpretation of searches for supersymmetry with simplified models*, [arXiv:1301.2175](#).